THE ASTRONOMICAL JOURNAL, 123:3277–3297, 2002 June

ABUNDANCES IN STARS FROM THE RED GIANT BRANCH TIP TO NEAR THE MAIN-SEQUENCE TURNOFF IN M71. III. ABUNDANCE RATIOS[1]

SOLANGE V. RAMÍREZ[2] AND JUDITH G. COHEN[2]

Received 2001 July 5; accepted 2002 February 15

ABSTRACT

We present abundance ratios for 23 elements with respect to Fe in a sample of stars with a wide range in luminosity, from luminous giants to stars near the turnoff in a globular cluster. Our sample of 25 stars in M71 includes 10 giant stars more luminous than the red horizontal branch (RHB), three HB stars, nine giant stars less luminous than the RHB, and three stars near the turnoff. The analyzed spectra, obtained with HIRES at the Keck Observatory, are of high dispersion ($R = \lambda/\Delta\lambda = 35{,}000$). We find that the neutron capture, the iron peak, and the $\alpha-$element abundance ratios show no trend with $T_{\rm eff}$ and low scatter around the mean between the top of the RGB and near the main-sequence turnoff. The α-elements Mg, Ca, Si, and Ti are overabundant relative to Fe. The anticorrelation between O and Na abundances observed in other metal-poor globular clusters is detected in our sample and extends to the main sequence. A statistically significant correlation between Al and Na abundances is observed among the M71 stars in our sample, extending to $M_V = +1.8$, fainter than the luminosity of the RGB bump in M5. Lithium is varying, as expected, and Zr may be varying from star to star as well. M71 appears to have abundance ratios very similar to M5, whose bright giants were studied by Ivans et al., but seems to have a smaller amplitude of star-to-star variations at a given luminosity, as might be expected from its higher metallicity. Neither extremely O-poor, Na-rich stars nor extremely O-rich, Na-poor, stars such as are observed in M5 and in M13, are present in our sample of M71 stars. The results of our abundance analysis of 25 stars in M71 provide sufficient evidence of abundance variations at unexpectedly low luminosities to rule out the mixing scenario. Either alone or, even more powerfully, combined with other recent studies of C and N abundances in M71 stars, the existence of such abundance variations cannot be reproduced within the context of our current understanding of stellar evolution.

Key words: globular clusters: general — globular clusters: individual (M71) — stars: abundances — stars: evolution

On-line material: machine-readable table

1. INTRODUCTION

Abundance determinations of stars in Galactic globular clusters can provide valuable information about important astrophysical processes, such as stellar evolution, stellar structure, Galactic chemical evolution, and the formation of the Milky Way. Surface stellar abundances of C, N, O, and often Na, Mg, and Al, are found to be variable among red giants within a globular cluster. The physical process responsible for these star-to-star element variations is still uncertain (see the reviews of Kraft 1994 and Pinsonneault 1997, as well as Cohen, Behr, & Briley 2001, hereafter Paper I).

In order to study the origin of the star-to-star abundance variations, we have started a program to determine chemical abundances of the nearer Galactic globular cluster stars. Paper I presents the sample of stars in M71, the nearest globular cluster reachable from the northern hemisphere, and the atmosphere parameters of the program stars. Our sample includes stars over a large range in luminosity—19 giant stars, three horizontal branch (HB) stars, and three stars near the main-sequence turnoff—in order to study in a consistent manner red giants, horizontal-branch stars, and stars at the main-sequence turnoff. Our second paper (Ramírez et al. 2001, hereafter Paper II) discusses the iron abundance in M71. We found that the [Fe/H] abundances from both Fe I ([Fe/H] $= -0.71 \pm 0.08$) and Fe II ([Fe/H] $= -0.84 \pm 0.12$) lines agree with each other and with earlier determinations (Cohen 1983; Gratton et al. 1986; Leep et al. 1987; Sneden et al. 1994). We also found that the [Fe/H] obtained from Fe I and Fe II lines is constant within the rather small uncertainties for this group of stars over the full range in effective temperature ($T_{\rm eff}$) and luminosity. In this third paper of this series, we present our results for abundances of 23 atomic species in our sample of M71 stars.

2. ATOMIC LINE PARAMETERS

The abundance analysis is done using a current version of the LTE spectral synthesis program MOOG (Sneden 1973). A line list specifying the wavelengths, excitation potentials, *gf*-values, damping constants, and equivalent widths for the observed lines is required. The provenance of the equivalent widths, *gf*-values, and damping constants is discussed below.

In addition, a model atmosphere for the $T_{\rm eff}$ and surface gravity [log (g)] appropriate for each star and a value for the microturbulent velocity (ξ) are also required for the abundance analysis. We use the grid of model atmospheres from Kurucz (1993b) with a metallicity of [Fe/H] $= -0.5$ dex,

[1] Some of the data presented herein were obtained at the W. M. Keck Observatory, which is operated as a scientific partnership among the California Institute of Technology, the University of California, and the National Aeronautics and Space Administration. The Observatory was made possible by the generous financial support of the W. M. Keck Foundation.

[2] Palomar Observatory, Mail Stop 105-24, California Institute of Technology, Pasadena, CA 91125.

TABLE 1
STELLAR PARAMETERS FOR THE M71 SAMPLE FROM PAPER I AND PAPER II[a]

ID[b]	$T_{\rm eff}$ (K)	log (g)	ξ (km s^{-1})	$N_{\rm FeI}$	[Fe/H]$_{\rm FeI}$	$N_{\rm FeII}$	[Fe/H]$_{\rm FeII}$
1-45	3950	0.90	1.45	187	-0.60 ± 0.03	5	-0.45 ± 0.06
I	4150	1.00	1.38	186	-0.63 ± 0.03	6	-0.66 ± 0.07
1-66	4250	1.35	1.35	179	-0.58 ± 0.03	6	-0.67 ± 0.09
1-64	4200	1.35	1.37	187	-0.61 ± 0.03	5	-0.52 ± 0.09
1-56	4525	1.60	1.26	127	-0.48 ± 0.03	2	-0.68 ± 0.13
1-95	4550	1.65	1.25	184	-0.59 ± 0.03	8	-0.74 ± 0.05
1-81	4550	1.75	1.25	180	-0.56 ± 0.03	6	-0.93 ± 0.05
1-1	4700	2.05	1.20	134	-0.59 ± 0.03	5	-0.76 ± 0.05
1-80[c,d]	5300	2.40	1.80	71	-0.64 ± 0.03	5	-0.93 ± 0.05
1-87[c]	5300	2.40	1.80	128	-0.56 ± 0.03	9	-0.84 ± 0.05
1-94[c]	5300	2.40	1.80	94	-0.73 ± 0.03	6	-0.82 ± 0.05
1-60	4900	2.30	1.13	119	-0.74 ± 0.03	6	-0.62 ± 0.05
1-59	4600	2.30	1.23	141	-0.70 ± 0.03	5	-0.58 ± 0.05
G53476_4543	4900	2.65	1.13	174	-0.61 ± 0.03	7	-0.76 ± 0.05
2-160	5100	2.70	1.07	145	-0.49 ± 0.03	5	-0.94 ± 0.08
G53447_4707	5175	2.75	1.04	155	-0.51 ± 0.03	7	-0.83 ± 0.05
G53445_4647	5050	2.85	1.08	112	-0.59 ± 0.03	6	-0.80 ± 0.05
G53447_4703	5000	3.00	1.10	125	-0.71 ± 0.03	4	-0.74 ± 0.05
G53425_4612	5150	3.15	1.05	80	-0.67 ± 0.03	2	-0.87 ± 0.07
G53477_4539	5150	3.15	1.05	119	-0.64 ± 0.03	5	-0.86 ± 0.05
G53457_4709	5200	3.35	1.03	93	-0.72 ± 0.03	5	-0.72 ± 0.12
G53391_4628	5100	3.35	1.07	106	-0.78 ± 0.03	5	-0.76 ± 0.05
G53417_4431	5800	4.05	0.83	38	-0.63 ± 0.04	3	-0.60 ± 0.12
G53392_4624	5800	4.05	0.83	36	-0.76 ± 0.03	3	-0.66 ± 0.08
G53414_4435	5900	4.15	0.80	13	-0.78 ± 0.05	2	-0.58 ± 0.16

[a] ξ and [Fe/H] have been slightly updated from the values given in Paper I.
[b] Identifications are from Arp & Hartwick (1971) or are assigned based on the J2000.0 coordinates, rh rm rs.s dd dm dd becoming Grmrss_dmdd.
[c] RHB star.
[d] Appears to show rotation (Paper I).

based on earlier high-dispersion iron-abundance analysis of M71 (Cohen 1983; Gratton et al. 1986; Leep et al. 1987; Sneden et al. 1994; Paper II). $T_{\rm eff}$ and log (g) are derived from the broadband photometry of the stars, as described in Paper I. The photometric $T_{\rm eff}$ has an error of $\pm$75 K for giants and $\pm$150 K for dwarfs and log (g) has an error of $\pm$0.2 dex. The microturbulent velocity is derived as described in Paper II; ξ has an error of $\pm$0.2 km s^{-1}. Table 1, reproduced from Paper II, lists the stellar parameters of our sample of M71 stars.

2.1. *Equivalent Widths*

The search for absorption features present in our HIRES data and the measurement of their equivalent width (W_λ) was done automatically with a FORTRAN code, EWDET, developed for this project. Details of this code and its features are described in Paper II. The line list identified and measured by EWDET is then correlated to the list of suitable unblended lines with atomic parameters to specifically identify the different atomic lines. The list of unblended atomic lines was created by inspection of the spectra of M71 stars, as well as the on-line solar spectrum taken with the Fourier transform spectrometer at the National Solar Observatory of Wallace, Hinkle, & Livingston (1998)[3] and the set of solar line identifications of Moore, Minnaert, & Houtgast (1966).

In Paper II we derived the λD-W_λ relation of the Fe I lines of "the weak line set" (Fe I lines within 2 σ levels of the λD-W_λ fit, $W_\lambda < 60$ mÅ, and errors less than a third of the W_λ). We used these λD-W_λ relations to determine "the good-line set" (lines with errors less than a third of the W_λ and with W_λ computed from the derived λD-W_λ relations). The W_λ of the lines presented in this paper are also determined using the fit to the λD-W_λ relation of the Fe I lines of the good-line set, except for the C I, O I, and Ca I lines, and for the elements that show hyperfine structure splitting (Sc II, V I, Mn I, Co I, Cu I, and Ba II). The equivalent widths of the C I and O I lines were measured by hand, since thermal motions become important at the low atomic weights of these elements and the λD-W_λ relations derived for Fe I lines may no longer be valid. For Ca I lines and the lines of elements that show hyperfine structure splitting, we used the equivalent widths measured automatically by EWDET but did not force them to fit the Fe I λD-W_λ relationship because of the probable different broadening mechanisms. Many of the Ca I lines were strong enough to be on the damping part of the curve of growth. The W_λ used in the abundance analysis are listed in Table 2 (available electronically), which also includes the W_λ for the Fe I and Fe II lines used in Paper II.

2.2. *Transition Probabilities*

Transition probabilities for the lines used in this analysis were obtained from the NIST Atomic Spectra Database (NIST Standard Reference Database No. 78; see Wiese et al. 1969; Martin et al. 1988; Fuhr et al. 1988; Wiese et al.

[3] At ftp://noao.edu.fts/visatl/README.

TABLE 2

EQUIVALENT WIDTHS (MÅ)

Ion	λ (Å)	χ (eV)	log (*gf*)	1–45	I	1–66	1–64	1–56	1–95	1–81	1–1	1–80	1–87	1–94	1–60	1–59	G53476 _4543	2–160	G53447 _4707	G53445 _4647	G53447 _4703	G53425 _4612	G53477 _4539	G53457 _4709	G53391 _4628	G53417 _4431	G53392 _4624	G53414 _4435
C I.....								...	30.0	...	...	...	...	...	...	...	...	24.3	...	16.1	...	...	...	...	...	...	...	...
C I.....	7115.170	8.640	−0.710	31.3	...	...	...	...	...	...	...	...	...	...	...	...	...	...	...	...	...	...	...	...	...	...	...	...
O I.....	6300.304	0.000	−9.780	76.2	73.8[a]	57.1	71.6	42.4[a]	44.9	44.5	30.5[a]	18.8[a]	23.4	20.1[a]	30.4	27.7[a]	25.3	15.2[a]	22.1	21.7[a]	...	...	14.1[a]	13.0[a]	...	...	...	...
O I.....	6363.776	0.020	−10.300	39.3	34.3	25.9	35.7	19.2[a]	19.6	22.3	...	...	...	9.0[a]	14.9[a]	16.0[a]	9.0	...	...	...	...	...	...	...	...	...	...	...
O I.....	7771.944	9.150	0.369	...	...	15.2[a]	21.3	23.2[a]	21.2	19.9	28.7	65.5	52.5	81.0	44.4	24.3[a]	28.8	19.2	37.5	27.9	27.9[a]	29.0[a]	27.2	26.2[a]	25.9[a]	32.9[a]	47.1[a]	71.7
O I.....	7774.166	9.150	0.223	...	17.2[a]	16.1[a]	18.8[a]	17.5[a]	23.8	17.5[a]	21.4[a]	63.6	50.9	62.3[a]	43.6[a]	26.8	22.8	19.0	33.5	27.9[a]	22.6[a]	31.8	27.9[a]	20.1	23.3	28.4[a]	34.6[a]	39.8[a]
O I.....	7775.388	9.150	0.001	...	18.6	...	14.3[a]	18.7[a]	14.7[a]	14.7[a]	14.3[a]	32.3	31.3	50.6[a]	32.5	15.5[a]	19.8	11.6	22.5[a]	23.5[a]	12.2[a]	16.6[a]	19.2	...	23.9[a]	28.2[a]	34.4[a]	48.7[a]
Na I....	5682.633	2.100	−0.700	159.9	130.6	137.0	123.8[a]	121.5	105.0	106.8	106.4	66.1[a]	68.6	63.1	64.4[a]	88.1	80.4	96.9	74.7	69.3	90.0	66.5[a]	66.6	57.4	69.0	47.2[a]	48.4	22.6[a]
Na I....	5688.193	2.100	−0.420	159.5	134.3	146.3	141.0	131.5	125.5	129.3	125.3	84.4	90.4	83.4	84.9	109.1	103.2	...	95.9	94.0	107.3	103.5	89.3	75.6	89.6	76.0	64.3	54.3[a]
Na I....	6154.225	2.100	−1.530	108.2	60.4	72.3	64.5	52.8	43.0	47.3	48.4	7.0[a]	15.7[a]	13.4[a]	18.4[a]	32.2	27.1	34.3	22.5	28.7	31.1	16.1[a]	13.7[a]	13.5[a]	28.1[a]	14.7[a]	...	...

NOTE.—Table 2 is presented in its entirety in the electronic edition of the Astronomical Journal. A portion is shown here for guidance regarding its form and content.

[a] Line identified by hand. All other lines are identified automatically.

TABLE 3
CORRECTION FACTORS FOR INVERTED SOLAR *gf*-VALUES

Ion (1)	No. of Common Lines between NIST and Solar (2)	Correction Factor[a] (dex) (3)
Mg I	4	+0.10
Al I	6	+0.21
Ca I	12	+0.33
Ti I	30	+0.05
Cr I	11	+0.05
Ni I	33	+0.05

[a] *gf*(used) = *gf*(Thevenin) + correction factor.

1996) when possible. Nearly 80% of the lines selected as suitable from the HIRES spectra have transition probabilities from the NIST database. For the remaining lines the *gf*-values come from the inverted solar analysis of Thévenin (1989, 1990), corrected by the factors listed in Table 3, which are needed to place both sets of transition probabilities onto the same scale. The correction factor was computed as the mean difference in log (*gf*) between the NIST and solar values for the lines in common, which number is given in column (2) of Table 3. Elements not listed in Table 3 have transition probabilities from the NIST database for all their lines utilized here.

Six elements show hyperfine structure splitting (Sc II, V I, Mn I, Co I, Cu I, and Ba II). The corresponding hyperfine structure constants were taken from Prochaska et al. (2000).

2.3. *Damping Constants*

Most of the Na I and Ca I lines are strong enough for damping effects to be important. For Na I the interaction constants, C_6, of the van de Waals broadening were taken from the solar analysis of Baumüller et al. (1998). Smith & Raggett (1981) studied collisional broadening of 17 Ca I lines. Comparing their experimental results and the predicted values of C_6 obtained using the Unsöld approximation, we found that the experimental C_6 are about 10 times larger than the Unsöld C_6. Thus for the Ca I we used the experimental C_6 from Smith & Raggett (1981) when available; otherwise we use 10 times the Unsöld approximation. The empirical values of C_6 for Al I and Mg I from Baumüller & Gehren (1996) and Zhao et al. (1998), respectively, are also used. We used 4 times the Unsöld approximation for those Al I lines without empirical damping constants. For the lines of all other ions we set C_6 to be twice the Unsöld approximation, as was done in Paper II for the Fe I lines following Holweger et al. (1991).

2.4. *Solar Abundances*

We need to establish the solar abundances corresponding to our adopted set of *gf*-values and damping constants. Solar abundance ratios were computed using our compilation of atomic parameters, the Kurucz model atmosphere for the Sun (Kurucz 1993b), and the list of equivalent widths from Moore et al. (1966). The results are listed in Table 4. The O abundance from the permitted lines is corrected by a factor of 0.35 dex (see below). There is a general agreement with the meteoric solar abundance ratios from Anders & Grevesse (1989). The difference between our solar abundances and the meteoric solar abundances from Anders & Grevesse (1989) is listed in column (5) of Table 4. This difference is within the standard deviation of our own measurements, with the exception of [Ca/Fe], which is our most deviant abundance ratio. The difference we found is almost the same as the correction factor applied to the solar *gf*-values listed in Table 3. We use these solar abundance ratios, derived from our choice of atomic line parameters, to compute the abundance ratios for our sample of M71 stars.

TABLE 4
SOLAR ABUNDANCE RATIOS [X/FE]

Ion (1)	No. of Lines (2)	[X/Fe][a] (dex) (3)	σ[a] (dex) (4)	Δ(us-meteoric)[b] (dex) (5)
Li I[c]	1	0.94	...	−0.22[d]
C I	4	+1.08	0.04	+0.03
O I	5	+1.53	0.10	+0.11
Na I	4	−1.30	0.09	−0.10
Mg I	10	+0.03	0.24	−0.05
Al I	6	−1.20	0.15	−0.17
Si I	20	+0.14	0.12	+0.09
K I	1	−2.28	...	+0.10
Ca I	15	−1.56	0.14	−0.39
Sc II	7	−4.26	0.12	+0.16
Ti I	40	−2.48	0.15	+0.09
V I	13	−3.55	0.14	−0.06
Cr I	12	−1.72	0.16	+0.10
Mn I	4	−2.09	0.12	−0.12
Co I	7	−2.60	0.08	0.00
Ni I	43	−1.19	0.18	+0.07
Cu I	1	−3.44	...	−0.20
Zn I	1	−2.94	...	−0.09
Y II	1	−4.96	...	+0.33
Zr I	4	−4.52	0.16	+0.38
Ba II	3	−5.29	0.08	+0.01
La II	3	−6.27	0.07	+0.04
Eu II	1	−6.96	...	+0.01

[a] Mean and 1 σ rms deviation about the mean for the abundance in the Sun of the lines of a particular ion using our adopted atomic line parameters.
[b] Meteoric solar abundances from Anders & Grevesse (1989).
[c] log ϵ(Li).
[d] The photospheric solar Li abundance from Anders & Grevesse (1989) is used.

2.5. *Non-LTE Effects*

The non-LTE treatment of the oxygen permitted lines is discussed in § 3. The K I resonance lines are strongly affected by non-LTE effects in the Sun (de la Reza & Muller 1975). Takeda et al. (2001) carried out statistical equilibrium calculations for the K I line 7699 Å, the only line used in our analysis for metal-poor stars. We applied a non-LTE correction to our results of *K* abundance following Takeda et al. (2001). The smallest correction applied was −0.12 dex for the cool giant stars, and the largest correction was −0.7 dex for the HB stars. Without these corrections a very strong dependence of *K* abundance on $T_{\rm eff}$ (equivalent to luminosity) was seen.

The aluminum lines are also affected by non-LTE in metal-poor stars (Baumüller & Gehren 1997). Unfortunately, the statistical equilibrium calculations of Baumüller

& Gehren (1997) included only dwarf stars. Their non-LTE corrections increase with decreasing metallicity and are larger for the 3961 Å line than for the 6697 Å doublet used in our analysis. Al and all other elements were treated assuming LTE.

3. ABUNDANCE ANALYSIS

Given the stellar parameters from Paper I, we determined the abundances using the equivalent widths obtained as described above. The abundance analysis is done using a current version of the LTE spectral synthesis program MOOG (Sneden 1973). We employ the grid of stellar atmospheres from Kurucz (1993b) to compute the abundances of C, O, Na, Mg, Al, Si, K, Ca, Sc, Ti, V, Cr, Mn, Co, Ni, Cu, Zn, Y, Zr, Ba, La, and Eu using the four stellar atmosphere models with the closest $T_{\rm eff}$ and log (g) to each star's parameters. The abundances were interpolated using results from the closest stellar model atmospheres to the appropriate $T_{\rm eff}$ and log (g) for each star.

We also determine the abundance of Li using a synthesis of the spectra in the area of the doublet at 6707 Å, which, since it is not well resolved, is considered as only one line in Table 5a. The Li abundance is given as $\log \epsilon(\mathrm{Li}) = \log (N_{\rm Li}/N_{\rm H}) + 12.0$, where N is the number of atoms. In this case, we used the stellar model atmosphere from Kurucz (1993b) with the closest $T_{\rm eff}$ and log (g) to each star's parameters.

The abundance ratios, with the exception of [C/Fe], [O/Fe], [Si/Fe], and [Zn/Fe], are computed using the iron abundance from Fe I lines of Paper I, as slightly updated in Table 1, and our solar abundance ratios from Table 4. Given their high excitation potentials, the abundance ratios for the C I, Si I, and Zn I lines were computed using the [Fe/H] from Fe II lines. In the $T_{\rm eff}$ range of our sample of stars, most of the iron is in the form of Fe II and most of the oxygen is in the form of O I, so both species behave similarly for small changes in the atmospheric parameters. For this reason, we computed the abundance ratio of O using the Fe II lines as well. The computed abundance ratios are listed in Tables 5a to 5e.

There are 11 stars with equivalent widths measured for both the two forbidden and the permitted O lines. The difference of the oxygen abundance ratio from forbidden and permitted lines for those 11 stars and the Sun is plotted against $T_{\rm eff}$ in Figure 1. A clear trend with $T_{\rm eff}$ is observed, which may come from the different excitation potential of the forbidden and the permitted lines or from non-LTE effects on the permitted lines. We tried applying the non-LTE corrections suggested by Gratton et al. (1999) and by Takeda et al. (2002) to the permitted lines, but the observed $T_{\rm eff}$ trend becomes even steeper. Meléndez et al. (2001) and Lambert (2002), among others, discuss the validity of the different oxygen abundance indicators. Since the forbidden lines are usually considered to give more reliable abundances (but see Israelian et al. 2001; Allende Prieto, Lambert, & Asplund 2001), we corrected the abundance ratio from the permitted lines by the amount given by the least-squares fit shown in Figure 1. The final [O/Fe] listed in Table 5a is the average for each star of the results from the forbidden and the corrected permitted lines. Note that a correction of 0.35 dex, which corresponds to the correction at the temperature of the Sun, was applied to the abundances deduced from the permitted lines of O I in the Sun to compute its [O/Fe] in the same way as for our M71 sample of stars.

The abundance ratios (absolute abundance for Li) for each star in our M71 sample are plotted against the photometric $T_{\rm eff}$ in Figures 2 to 7. The error bars shown in Figures

TABLE 5a
ABUNDANCE RATIOS: LI-NA

Star	$N_{\rm Li}$	[Li/Fe]	$N_{\rm C}$	[C/Fe]	$N_{\rm O}$	[O /Fe]	$N_{\rm Na}$	[Na/Fe]
1-45	0	...	2	2.10 ± 0.12	2	−0.19 ± 0.07	4	0.57 ± 0.08
I	0	...	1	1.20 ± 0.10	4	0.20 ± 0.18	4	0.22 ± 0.08
1-66	1	<−0.61	1	1.93 ± 0.11	4	0.03 ± 0.08	4	0.41 ± 0.07
1-64	1	<−0.79	0	...	5	0.14 ± 0.07	4	0.25 ± 0.05
1-56	0	...	0	...	5	0.01 ± 0.10	4	0.34 ± 0.08
1-95	1	<−0.39	1	1.32 ± 0.09	5	0.09 ± 0.11	4	0.23 ± 0.08
1-81	0	...	0	...	5	0.27 ± 0.14	4	0.27 ± 0.07
1-1	1	<0.36	0	...	4	0.10 ± 0.07	4	0.39 ± 0.06
1-80	1	<−0.69	0	...	4	0.53 ± 0.19	4	0.03 ± 0.12
1-87	0	...	0	...	4	0.34 ± 0.07	4	0.10 ± 0.05
1-94	1	<−0.69	0	...	5	0.53 ± 0.21	4	0.12 ± 0.08
1-60	0	...	0	...	5	0.33 ± 0.12	4	0.04 ± 0.05
1-59	0	...	0	...	5	0.15 ± 0.12	4	0.11 ± 0.05
G53476_4543	0	...	0	...	5	0.26 ± 0.07	4	0.15 ± 0.05
2-160	1	< 0.61	1	1.05 ± 0.11	4	0.06 ± 0.14	3	0.34 ± 0.08
G53447_4707	1	1.01 ± 0.10	0	...	4	0.33 ± 0.07	4	0.14 ± 0.05
G53445_4647	1	0.99 ± 0.10	1	0.74 ± 0.09	4	0.31 ± 0.09	4	0.16 ± 0.05
G53447_4703	0	...	0	...	3	0.11 ± 0.10	4	0.37 ± 0.05
G53425_4612	1	1.29 ± 0.10	0	...	3	0.34 ± 0.12	4	0.21 ± 0.09
G53477_4539	0	...	0	...	4	0.33 ± 0.07	4	0.06 ± 0.07
G53457_4709	0	...	0	...	3	0.14 ± 0.11	4	0.10 ± 0.06
G53391_4628	0	...	0	...	3	0.32 ± 0.13	4	0.27 ± 0.05
G53417_4431	0	...	0	...	3	0.12 ± 0.11	4	0.28 ± 0.07
G53392_4624	0	...	0	...	3	0.37 ± 0.09	3	0.19 ± 0.10
G53414_4435	0	...	0	...	3	0.54 ± 0.18	3	0.14 ± 0.14

TABLE 5b

ABUNDANCE RATIOS: MG-CA

Star	N_{Mg}	[Mg/Fe]	N_{Al}	[Al/Fe]	N_{Si}	[Si/Fe]	N_{K}	[K/Fe]	N_{Ca}	[Ca/Fe]
1-45	8	0.43 ± 0.09	3	0.45 ± 0.09	12	0.04 ± 0.07	1	−0.71 ± 0.09	15	0.32 ± 0.07
I	8	0.46 ± 0.06	3	0.28 ± 0.11	14	0.18 ± 0.08	1	−0.12 ± 0.09	13	0.42 ± 0.06
1-66	9	0.47 ± 0.09	3	0.26 ± 0.07	17	0.22 ± 0.10	1	0.03 ± 0.09	14	0.39 ± 0.06
1-64	8	0.41 ± 0.09	4	0.19 ± 0.07	16	0.15 ± 0.10	1	−0.82 ± 0.09	15	0.39 ± 0.06
1-56	4	0.33 ± 0.06	0	...	10	0.34 ± 0.14	0	...	10	0.43 ± 0.07
1-95	9	0.44 ± 0.09	3	0.13 ± 0.07	17	0.36 ± 0.06	1	−0.17 ± 0.09	13	0.42 ± 0.06
1-81	9	0.46 ± 0.09	4	0.27 ± 0.07	16	0.42 ± 0.06	1	0.03 ± 0.09	14	0.47 ± 0.06
1-1	6	0.33 ± 0.11	1	0.27 ± 0.07	14	0.27 ± 0.06	1	−0.06 ± 0.09	12	0.55 ± 0.06
1-80	2	0.35 ± 0.06	0	...	10	0.47 ± 0.06	0	...	10	0.52 ± 0.13
1-87	6	0.35 ± 0.06	0	...	16	0.45 ± 0.06	0	...	12	0.47 ± 0.08
1-94	3	0.39 ± 0.13	2	0.11 ± 0.07	13	0.41 ± 0.06	1	−0.02 ± 0.09	10	0.42 ± 0.06
1-60	3	0.47 ± 0.06	0	...	12	0.20 ± 0.06	0	...	11	0.47 ± 0.06
1-59	4	0.43 ± 0.06	0	...	16	0.16 ± 0.06	0	...	12	0.44 ± 0.06
G53476_4543	5	0.36 ± 0.06	0	...	18	0.27 ± 0.06	0	...	15	0.41 ± 0.06
2-160	7	0.33 ± 0.08	2	0.17 ± 0.07	17	0.45 ± 0.09	0	...	13	0.48 ± 0.06
G53447_4707	7	0.32 ± 0.06	2	0.21 ± 0.12	17	0.38 ± 0.06	1	−0.19 ± 0.09	12	0.48 ± 0.06
G53445_4647	4	0.24 ± 0.06	1	0.39 ± 0.07	13	0.28 ± 0.06	0	...	12	0.44 ± 0.07
G53447_4703	3	0.44 ± 0.06	0	...	16	0.23 ± 0.06	1	0.19 ± 0.09	13	0.36 ± 0.06
G53425_4612	5	0.39 ± 0.16	0	...	4	0.14 ± 0.10	1	0.00 ± 0.09	9	0.47 ± 0.06
G53477_4539	6	0.43 ± 0.06	0	...	17	0.30 ± 0.06	0	...	11	0.38 ± 0.06
G53457_4709	4	0.45 ± 0.10	0	...	11	0.11 ± 0.13	0	...	11	0.50 ± 0.07
G53391_4628	2	0.13 ± 0.06	0	...	15	0.17 ± 0.06	0	...	10	0.39 ± 0.06
G53417_4431	1	0.16 ± 0.06	0	...	5	0.02 ± 0.13	0	...	11	0.40 ± 0.06
G53392_4624	1	0.39 ± 0.06	0	...	4	−0.01 ± 0.12	0	...	8	0.37 ± 0.07
G53414_4435	0	...	0	...	0	...	0	...	8	0.42 ± 0.10

TABLE 5c

ABUNDANCE RATIOS: SC-CR

Star	N_{Sc}	[Sc/Fe]	N_{Ti}	[Ti/Fe]	N_{V}	[V/Fe]	N_{Cr}	[Cr/Fe]
1-45	6	0.23 ± 0.08	36	0.34 ± 0.06	14	0.43 ± 0.12	10	−0.03 ± 0.08
I	7	0.29 ± 0.21	37	0.23 ± 0.05	14	0.18 ± 0.15	9	−0.10 ± 0.08
1-66	6	0.21 ± 0.07	38	0.23 ± 0.05	13	0.03 ± 0.07	9	−0.11 ± 0.07
1-64	7	0.19 ± 0.12	37	0.25 ± 0.05	14	0.19 ± 0.15	8	−0.10 ± 0.07
1-56	4	−0.04 ± 0.12	21	0.15 ± 0.07	9	0.08 ± 0.14	3	−0.21 ± 0.13
1-95	6	0.15 ± 0.06	36	0.06 ± 0.04	14	0.02 ± 0.08	9	−0.23 ± 0.07
1-81	7	0.07 ± 0.07	34	0.34 ± 0.05	14	0.36 ± 0.12	9	−0.07 ± 0.07
1-1	7	0.20 ± 0.19	25	0.22 ± 0.05	14	0.19 ± 0.07	5	−0.14 ± 0.07
1-80	4	−0.36 ± 0.15	8	0.17 ± 0.04	1	−0.05 ± 0.07	1	0.09 ± 0.07
1-87	7	−0.17 ± 0.06	16	0.13 ± 0.04	10	0.20 ± 0.07	4	−0.21 ± 0.07
1-94	6	−0.02 ± 0.06	5	0.07 ± 0.04	4	0.03 ± 0.07	3	−0.35 ± 0.10
1-60	5	0.20 ± 0.07	10	0.03 ± 0.06	3	−0.25 ± 0.18	3	−0.19 ± 0.14
1-59	5	0.26 ± 0.06	23	0.13 ± 0.04	11	0.06 ± 0.07	7	−0.11 ± 0.07
G53476_4543	6	0.14 ± 0.06	32	0.20 ± 0.04	11	0.16 ± 0.07	9	−0.15 ± 0.07
2-160	6	0.03 ± 0.06	24	0.27 ± 0.05	12	0.17 ± 0.07	7	−0.08 ± 0.08
G53447_4707	7	−0.07 ± 0.07	21	0.16 ± 0.04	9	0.09 ± 0.07	8	−0.18 ± 0.07
G53445_4647	7	−0.02 ± 0.06	15	0.20 ± 0.04	8	0.18 ± 0.08	6	−0.10 ± 0.07
G53447_4703	7	0.29 ± 0.21	17	0.21 ± 0.04	6	0.05 ± 0.08	6	−0.06 ± 0.07
G53425_4612	5	0.06 ± 0.13	6	0.23 ± 0.05	7	0.08 ± 0.07	3	−0.15 ± 0.12
G53477_4539	5	0.02 ± 0.06	13	0.19 ± 0.04	7	0.15 ± 0.09	3	−0.23 ± 0.13
G53457_4709	6	−0.07 ± 0.06	8	0.23 ± 0.04	3	0.09 ± 0.07	3	−0.12 ± 0.08
G53391_4628	6	0.10 ± 0.06	15	0.30 ± 0.04	0	...	3	−0.18 ± 0.07
G53417_4431	3	−0.21 ± 0.06	6	0.27 ± 0.07	0	...	1	−0.17 ± 0.07
G53392_4624	3	0.09 ± 0.11	6	0.06 ± 0.09	0	...	0	...
G53414_4435	1	0.15 ± 0.07	4	0.15 ± 0.16	0	...	0	...

TABLE 5d

ABUNDANCE RATIOS: MN-ZN

Star	N_{Mn}	[Mn/Fe]	N_{Co}	[Co/Fe]	N_{Ni}	[Ni/Fe]	N_{Cu}	[Cu/Fe]	N_{Zn}	[Zn/Fe]
1−45	3	−0.28 ± 0.22	7	0.09 ± 0.08	37	0.09 ± 0.05	1	−0.12 ± 0.09	0	...
I	4	−0.24 ± 0.06	7	0.02 ± 0.07	35	0.05 ± 0.05	1	0.05 ± 0.09	0	...
1−66	4	−0.25 ± 0.06	7	0.01 ± 0.05	35	0.06 ± 0.05	1	0.14 ± 0.09	1	0.74 ± 0.12
1−64	4	−0.39 ± 0.06	8	0.02 ± 0.05	38	0.08 ± 0.05	1	−0.22 ± 0.09	1	0.64 ± 0.12
1−56	0	...	3	0.00 ± 0.05	29	0.04 ± 0.06	0	...	0	...
1−95	4	−0.36 ± 0.06	7	−0.02 ± 0.06	37	0.03 ± 0.05	1	0.12 ± 0.09	0	...
1−81	4	−0.16 ± 0.06	7	0.04 ± 0.05	36	0.00 ± 0.05	1	0.12 ± 0.09	0	...
1−1	4	−0.27 ± 0.06	6	0.04 ± 0.06	29	0.02 ± 0.06	1	0.07 ± 0.09	0	...
1−80	0	...	0	...	17	−0.07 ± 0.06	1	0.38 ± 0.09	0	...
1−87	4	−0.24 ± 0.09	4	0.13 ± 0.08	27	−0.07 ± 0.05	1	0.16 ± 0.09	1	0.46 ± 0.09
1−94	3	−0.31 ± 0.06	0	...	16	0.00 ± 0.06	1	0.09 ± 0.09	1	0.44 ± 0.09
1−60	0	...	2	0.04 ± 0.12	19	0.00 ± 0.05	1	−0.30 ± 0.09	0	...
1−59	0	...	3	0.03 ± 0.07	28	0.07 ± 0.05	1	0.04 ± 0.09	0	...
G53476_4543	0	...	3	0.05 ± 0.05	36	−0.02 ± 0.05	1	0.07 ± 0.09	0	...
2−160	3	−0.28 ± 0.06	7	0.12 ± 0.05	28	−0.03 ± 0.06	1	0.14 ± 0.09	1	0.42 ± 0.11
G53447_4707	3	−0.27 ± 0.06	4	−0.05 ± 0.08	34	−0.05 ± 0.05	1	0.00 ± 0.09	1	0.44 ± 0.09
G53445_4647	0	...	2	0.00 ± 0.17	23	0.00 ± 0.07	1	0.19 ± 0.09	1	0.34 ± 0.09
G53447_4703	2	0.05 ± 0.12	1	0.04 ± 0.05	25	0.05 ± 0.05	1	0.15 ± 0.09	0	...
G53425_4612	2	−0.20 ± 0.10	0	...	13	0.02 ± 0.10	1	0.08 ± 0.09	0	...
G53477_4539	0	...	0	...	24	−0.03 ± 0.06	1	0.09 ± 0.09	0	...
G53457_4709	0	...	0	...	15	−0.01 ± 0.07	1	−0.01 ± 0.09	1	0.20 ± 0.14
G53391_4628	0	...	2	0.14 ± 0.15	20	−0.03 ± 0.07	1	0.15 ± 0.09	0	...
G53417_4431	0	...	0	...	7	−0.10 ± 0.14	0	...	0	...
G53392_4624	0	...	0	...	5	−0.20 ± 0.15	0	...	0	...
G53414_4435	0	...	0	...	2	−0.01 ± 0.06	0	...	0	...

TABLE 5e

ABUNDANCE RATIOS: Y-EU

Star	N_{Y}	[Y/Fe]	N_{Zr}	[Zr/Fe]	N_{Ba}	[Ba/Fe]	N_{La}	[La/Fe]	N_{Eu}	[Eu/Fe]
1−45	0	...	3	0.09 ± 0.27	3	0.25 ± 0.14	2	0.22 ± 0.08	1	0.58 ± 0.09
I	1	−0.16 ± 0.09	4	−0.24 ± 0.10	3	0.35 ± 0.08	1	0.15 ± 0.08	1	0.46 ± 0.09
1−66	0	...	4	−0.30 ± 0.13	3	0.33 ± 0.09	3	0.20 ± 0.08	1	0.38 ± 0.09
1−64	0	...	3	−0.23 ± 0.08	2	0.31 ± 0.08	2	0.32 ± 0.12	1	0.49 ± 0.09
1−56	0	...	1	−0.57 ± 0.08	3	0.52 ± 0.20	2	0.27 ± 0.24	1	0.02 ± 0.09
1−95	1	−0.26 ± 0.09	3	−0.38 ± 0.08	3	0.49 ± 0.09	2	0.09 ± 0.08	1	0.32 ± 0.09
1−81	0	...	2	0.00 ± 0.08	3	0.34 ± 0.12	2	0.27 ± 0.12	1	0.26 ± 0.09
1−1	0	...	0	...	2	0.18 ± 0.09	1	0.21 ± 0.08	0	...
1−80	0	...	0	...	3	0.38 ± 0.37	0	...	1	0.15 ± 0.09
1−87	0	...	1	0.20 ± 0.08	3	0.08 ± 0.18	0	...	1	0.20 ± 0.09
1−94	0	...	0	...	3	0.29 ± 0.21	1	0.24 ± 0.08	0	...
1−60	0	...	0	...	3	0.55 ± 0.08	0	...	0	...
1−59	0	...	0	...	3	0.38 ± 0.16	1	0.31 ± 0.08	0	...
G53476_4543	0	...	1	−0.12 ± 0.08	3	0.23 ± 0.16	1	0.19 ± 0.08	1	0.33 ± 0.09
2−160	0	...	1	0.22 ± 0.08	3	0.25 ± 0.17	1	0.12 ± 0.08	0	...
G53447_4707	1	−0.23 ± 0.09	0	...	3	0.26 ± 0.17	1	−0.02 ± 0.08	1	0.25 ± 0.09
G53445_4647	0	...	0	...	2	0.35 ± 0.20	0	...	0	...
G53447_4703	0	...	0	...	3	0.15 ± 0.19	0	...	0	...
G53425_4612	0	...	0	...	3	0.41 ± 0.09	0	...	0	...
G53477_4539	0	...	0	...	3	0.22 ± 0.16	1	0.41 ± 0.08	0	...
G53457_4709	0	...	0	...	3	0.22 ± 0.19	0	...	0	...
G53391_4628	0	...	0	...	3	0.33 ± 0.23	0	...	0	...
G53417_4431	0	...	0	...	3	0.22 ± 0.13	0	...	0	...
G53392_4624	0	...	0	...	2	0.61 ± 0.32	0	...	0	...
G53414_4435	0	...	0	...	3	0.33 ± 0.09	0	...	0	...

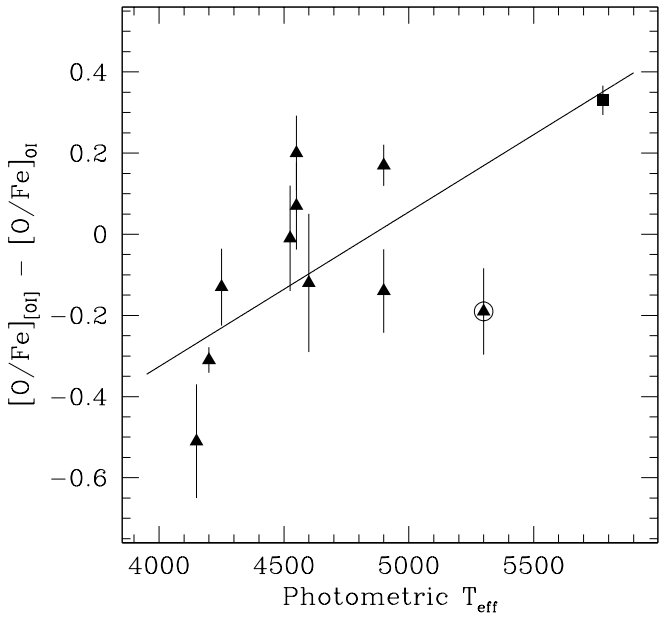

FIG. 1.—Difference between the oxygen abundance ratio from the forbidden and permitted lines shown as a function of $T_{\rm eff}$. The solid line is a linear fit weighted by the errors. The O abundances subsequently deduced from the permitted lines are corrected by the linear fit shown here. The RHB stars are marked with open circles, while the position of the Sun is indicated by a filled square.

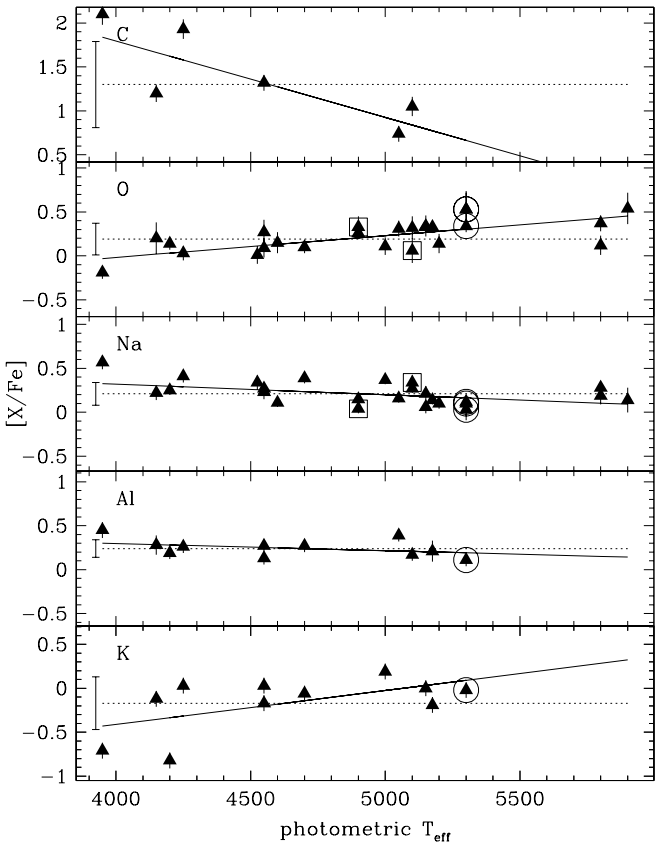

FIG. 3.—Abundance ratios of C, O, Na, Al, and K with respect to Fe against $T_{\rm eff}$. The solid line is a linear fit weighted by the errors. The dashed line indicates the mean abundance ratio with its respective error plotted as an error bar at 3925 K. The RHB stars are marked by open circles. A non-LTE correction has been applied to the O I permitted lines and the K I line. The C abundances determined from C I lines in the cooler M71 stars are believed to be spurious due to contamination by lines from the red system of CN (see text). Stars 1-60 and 2-160, part of whose spectra are shown in Fig. 10, are marked with open squares in the [O/Fe] and [Na/Fe] panels.

2 to 7 correspond to the standard deviation of results of different atomic lines divided by the square root of the number of lines used for each star. The solid line shown in Figures 3 to 7 is a linear fit weighted by the errors of the respective abundance ratio versus $T_{\rm eff}$. The dashed line shown in these figures indicates the mean abundance ratio and its respective error plotted as an error bar at 3925 K. The error in the mean abundance ratio corresponds to the standard deviation within our sample of stars divided by the square root of the number of stars for which an abundance was derived for that ion.

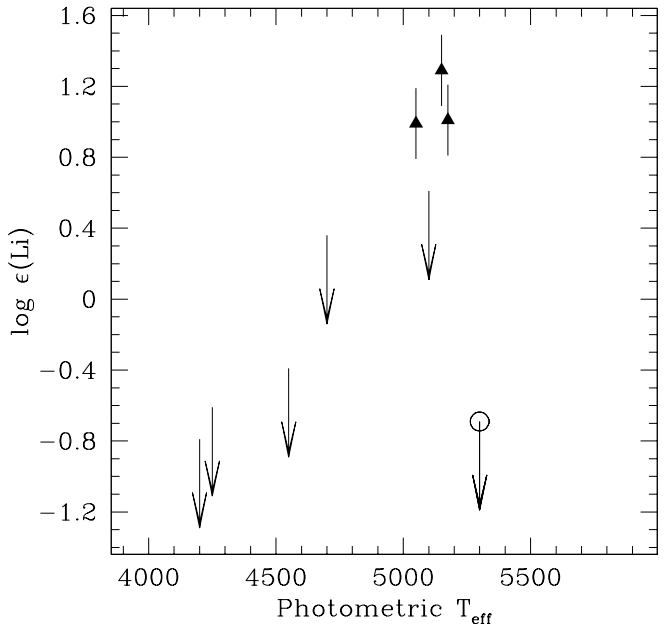

FIG. 2.—log ϵ(Li) against $T_{\rm eff}$. The RHB stars are marked by open circles. Arrows represent upper limits for the strength of the Li I line.

We estimate the sensitivity of the abundances with respect to small changes in the equivalent widths (synthesis for Li) and the stellar parameters in four cases: 4000/1.0/1.4, 4250/1.0/1.4, 5000/2.5/1.0, and 5500/4.0/0.6, where the three numbers correspond to $T_{\rm eff}$/log (g)/ξ. The case 4000/1.0/1.4 has been computed only for elements with high-excitation lines, which are more sensitive at lower temperatures. The stellar parameters of these cases span the relevant range of atmospheric parameters for our M71 sample. We estimated the error in the W_λ to be 10% for all the lines.

The error of the synthesis of the Li doublet is estimated to be $\pm$0.1 dex. The results are listed in Table 6, where the range adopted for each parameter is representative of its uncertainty.

Because of the high excitation of the C I lines studied here, this is the ion included in our analysis whose derived abundance is most sensitive to $T_{\rm eff}$. [Ca/H] also has a sensitive dependence on $T_{\rm eff}$ and on ξ, because the Ca I lines are all rather strong and have large damping constants.

The mean abundance ratios and their errors are listed in Table 7. The statistical error, $\sigma_{\rm obs}$, corresponds to the standard deviation of sample of stars divided by the square root

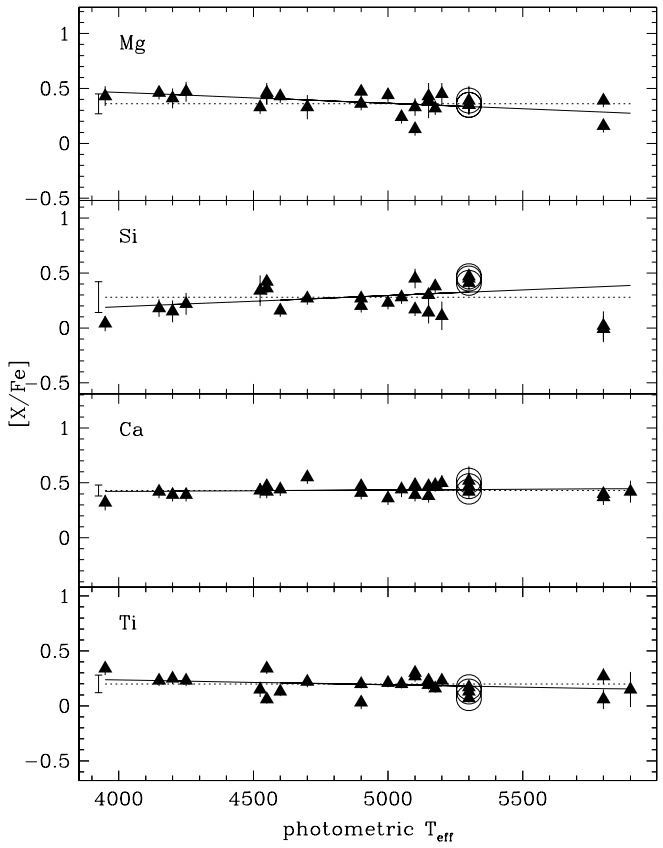

FIG. 4.—Abundance ratios of the α-elements Mg, Si, Ca, and Ti with respect to Fe against $T_{\rm eff}$. The symbols are the same as in Fig. 3.

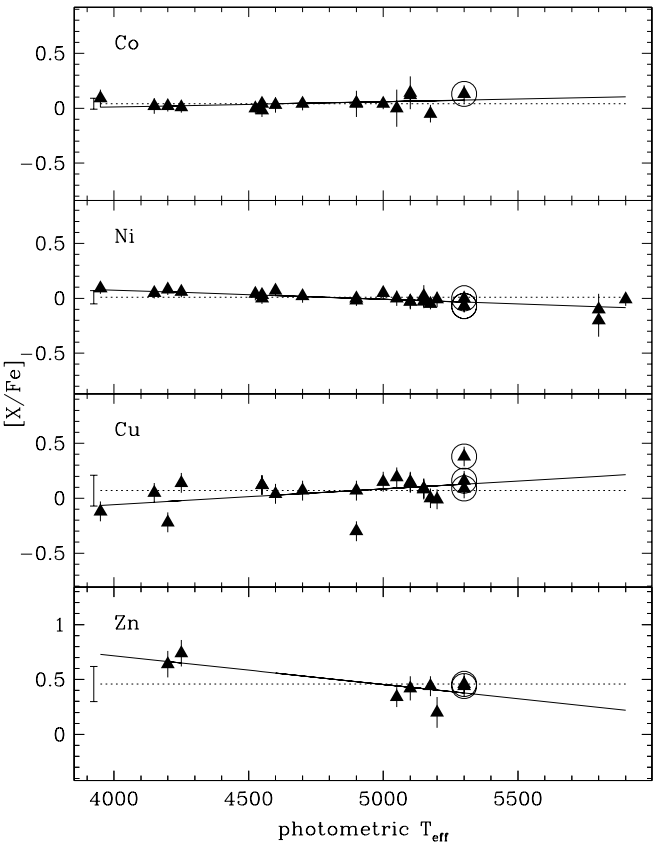

FIG. 6.—Abundance ratios of the iron peak elements Co, Ni, Cu, and Zn with respect to Fe against $T_{\rm eff}$. The symbols are the same as in Fig. 3.

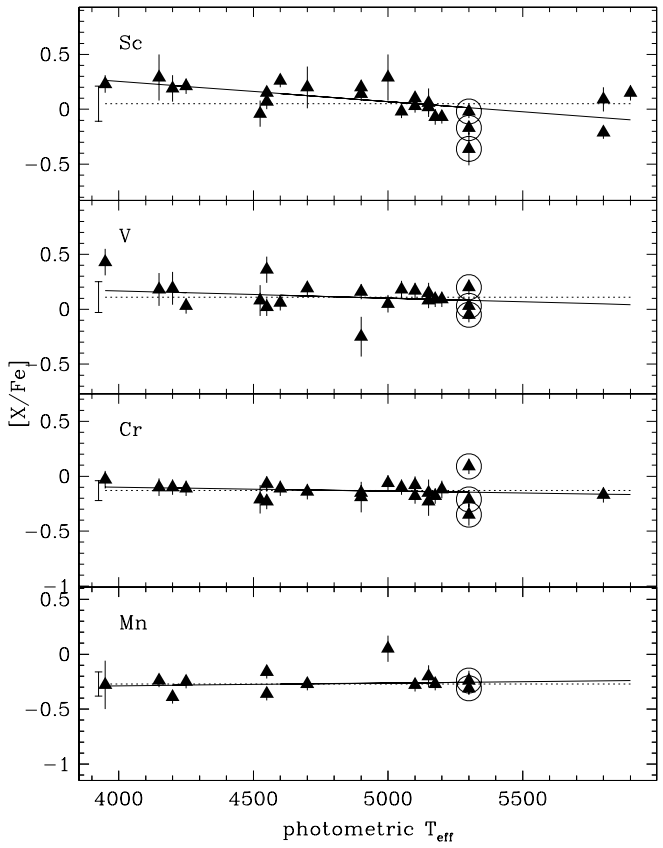

FIG. 5.—Abundance ratios of the iron peak elements Sc, V, Cr, and Mn with respect to Fe against $T_{\rm eff}$. The symbols are the same as in Fig. 3.

of the number of stars, and it is a measure of the scatter of the abundance ratio in the sample of M71 stars. In order to quantify the abundance ratio variations within our sample of M71 stars, we have to compare the measure of the scatter with the predicted error from the stellar parameters and the measurement of the W_λ (or synthesis for Li). We estimated the predicted error, $\sigma_{\rm pred}$, using the following equation:

$$\begin{aligned}\sigma^2_{\rm pred}([{\rm X/Fe}]) = {} & \Delta({\rm X}:W_\lambda)^2/N_{\rm lines}({\rm X}) \\ & + \Delta({\rm Fe}:W_\lambda)^2/N_{\rm lines}({\rm Fe}) \\ & + [\Delta({\rm X}:T_{\rm eff}) - \Delta({\rm Fe}:T_{\rm eff})]^2 \\ & + \{\Delta[{\rm X}:\log(g)] - \Delta[{\rm Fe}:\log(g)]\}^2 \\ & + [\Delta({\rm X}:\xi) - \Delta({\rm Fe}:\xi)]^2 \\ & + \{\Delta({\rm X}:[{\rm Fe/H}]) - \Delta({\rm Fe}:[{\rm Fe/H}])\}^2,\end{aligned}$$

where $\Delta({\rm X}:W_\lambda)$, $\Delta({\rm X}:T_{\rm eff})$, $\Delta[{\rm X}:\log(g)]$, $\Delta({\rm X}:\xi)$, and $\Delta({\rm X}:[{\rm Fe/H}])$ are listed in columns (2), (3), (4), (5), and (6) of Table 6. $N_{\rm lines}$ is the number of lines used to compute the abundances, X denotes the element under consideration, and Fe denotes either Fe I or Fe II, whichever was used to compute the abundance ratio. Our $\sigma_{\rm pred}$ ignores covariance among the error terms, which is discussed in detail by Johnson (2002). She shows that these additional terms are fairly small, and they will be even smaller in our case, as we have determined $\log(g)$ using isochrones rather than through ionization equilibria (see Paper I). The general small trends seen in Figures 2 to 7 of [X/Fe] slightly increasing toward

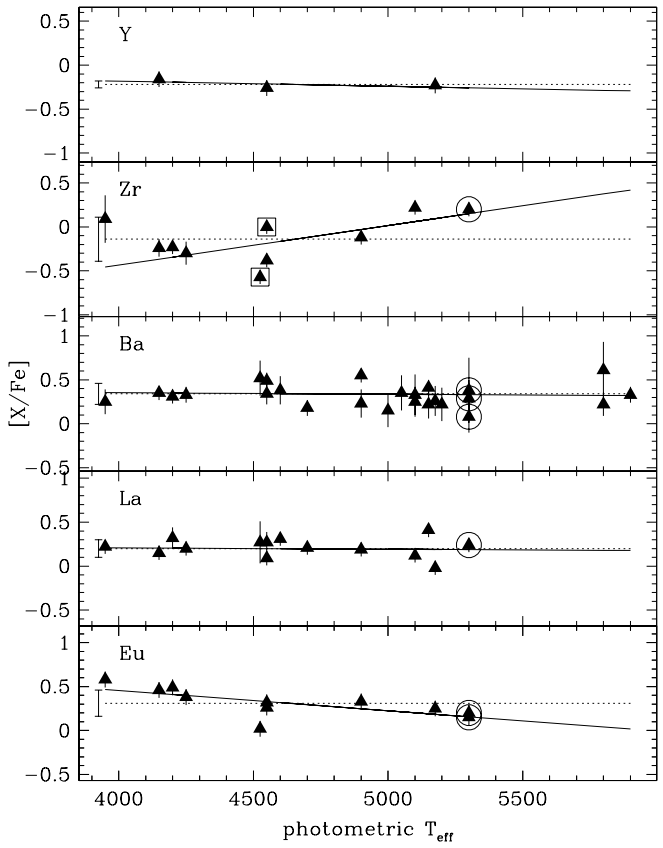

FIG. 7.—Abundance ratios of the neutron-capture elements Y, Zr, Ba, La, and Eu with respect to Fe against $T_{\rm eff}$. The symbols are the same as in Fig. 3. Stars 1-56 and 1-81, part of whose spectra are shown in Fig. 9, are marked with open squares in the [Zr/Fe] panel.

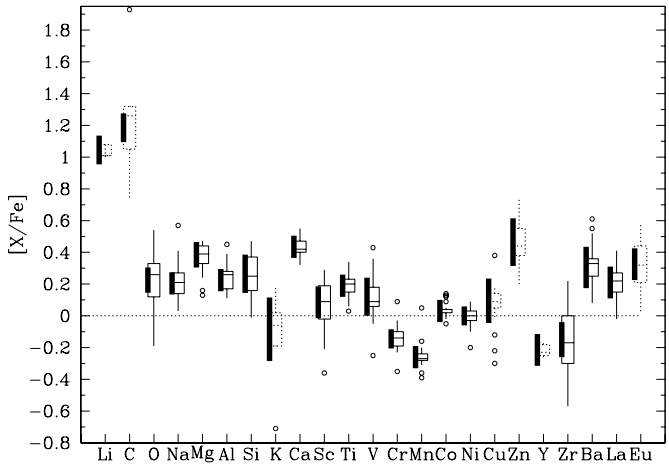

FIG. 8.—Summary of abundance ratios. Each abundance ratio is plotted with a box, of which the central horizontal line is the median abundance ratio, the bottom and the top show its interquartile range, the vertical lines coming out of the box mark the position of the adjacent points of the sample, and the outliers are plotted as open circles. Boxes constructed with dashed lines denote elements where only one line per star was observed. The thick line on the left side of the box is the predicted error (expected for the interquartile range), which included the dependence on the stellar parameters and the equivalent width determination.

cooler $T_{\rm eff}$ may result from ignoring the covariance terms (see Johnson 2002).

The predicted errors for each ion are listed in column (4) of Table 7. The maximum abundance trend over the relevant $T_{\rm eff}$ range for each element, $\Delta_{\rm max}$, is also listed in column (6) of Table 7. This parameter, which is not sensitive to star-to-star scatter abundance variations for stars at a given evolutionary state, is the slope of the linear fit of the abundance ratio versus $T_{\rm eff}$ times the range in $T_{\rm eff}$; its error is the error in the slope time the range in $T_{\rm eff}$ covered by the sample of stars in which the ion of interest was observed. The values of $\Delta_{\rm max}$ for essentially all elements observed are gratifyingly small, providing evidence to support many of the assumptions made in the course of this analysis, such as that of non-LTE.

A summary of the abundance ratios for our M71 sample is shown in Figure 8. The results for each element are depicted as a box whose central horizontal line is the median abundance ratio for all the M71 stars included, while the bottom and the top shows its interquartile range, the vertical lines coming out of the box mark the position of the adjacent points of the sample, and the outliers are plotted as open circles. The boxes drawn with dotted lines correspond to elements with abundances computed from only one line in each star and hence are more uncertain. The thick line on the left side of the box is the predicted 1 σ rms error scaled to correspond to the $\pm$25% interquartile range. As seen in Figure 8, the elements where we expect to see star-to-star variations in our M71 sample are O, Na, Zr, and the special cases of Li and C, each to be discussed in detail later.

4. DISCUSSION

4.1. Fe *Peak Elements*

The abundance ratios of [Sc/Fe], [V/Fe], [Cr/Fe], [Mn/Fe], [Co/Fe], and [Ni/Fe] follow the behavior of iron, as expected, showing no significant trend with $T_{\rm eff}$ and less scatter around the mean than the predicted error. The mean abundance ratios of Sc ($\langle$[Sc/Fe]$\rangle = +0.05 \pm 0.16$), V ($\langle$[V/Fe]$\rangle = +0.11 \pm 0.14$), and Ni ($\langle$[Ni/Fe]$\rangle = +0.01 \pm 0.06$) are consistent with the earlier results of Sneden et al. (1994), who analyzed high-resolution spectra of 10 giant stars in M71, obtaining $\langle$[Sc/Fe]$\rangle = +0.10 \pm 0.03$, $\langle$[V/Fe]$\rangle = +0.19 \pm 0.04$, and $\langle$[Ni/Fe]$\rangle = +0.07 \pm 0.04$. Our abundance ratios of the iron peak elements are also consistent with the results of Leep et al. (1987).

The Zn I line at 6362.3 Å is definitely present in the best of the spectra of the M71 giants, but is somewhat blended with the much stronger Fe I line at 6362.9 Å. In addition, the continuum there is depressed due to a broad autoionization Ca I feature. The rather high abundance of Zn we deduce must thus be regarded as quite uncertain until a full spectral synthesis of this region becomes available.

4.2. *Neutron-Capture Elements*

We have detected lines of the neutron-capture elements Y, Zr, Ba, La, and Eu. Cameron (1982) and Käppeler et al. (1989) analyzed the solar system meteoritic abundances of neutron-capture elements to yield accurate breakdowns into *r*- and *s*-process parts for each isotope, which have been summed into fractions for each element by Burris et al. (2000). At [Fe/H] < -2.0, as reviewed by Sneden et al. (2001), Zr, Ba, and La are neutron-capture elements synthesized through *s*-process reactions that occur mainly in low-

TABLE 6

SENSITIVITY OF ABUNDANCE

Stellar Parameters (1)	ΔW_λ (10%) (2)	$\Delta T_{\rm eff}$ (+100 K) (3)	$\Delta \log(g)$ (+0.2 dex) (4)	$\Delta\xi$ (+0.2 km s^{-1}) (5)	Δ[Fe/H] (+0.2 dex) (6)
Li I:					
5000/2.5/1.0.....	0.10[a]	0.13	0.01	0.00	0.01
C I:					
4250/1.0/1.4.....	0.10	−0.28	0.09	−0.02	−0.03
5000/2.5/1.0.....	0.07	−0.20	0.09	−0.01	0.00
5500/4.0/0.6.....	0.07	−0.11	0.07	0.00	0.00
O I:					
4250/1.0/1.4.....	0.08	−0.12	0.09	−0.01	−0.03
5000/2.5/1.0.....	0.06	−0.06	0.08	−0.01	−0.02
Na I:					
4250/1.0/1.4.....	0.17	0.09	−0.01	−0.07	0.01
5000/2.5/1.0.....	0.11	0.07	−0.01	−0.03	0.01
5500/4.0/0.6.....	0.10	0.06	−0.01	0.00	0.00
Mg I:					
4250/1.0/1.4.....	0.12	0.01	0.00	−0.04	0.00
5000/2.5/1.0.....	0.10	0.05	−0.01	−0.03	0.00
5500/4.0/0.6.....	0.16	0.06	−0.03	−0.02	0.00
Al I:					
4250/1.0/1.4.....	0.09	0.07	0.00	−0.03	0.00
5000/2.5/1.0.....	0.06	0.06	0.00	−0.01	0.01
Si I:					
4250/1.0/1.4.....	0.09	−0.12	0.06	−0.03	−0.04
5000/2.5/1.0.....	0.10	−0.07	0.05	−0.03	−0.04
5500/4.0/0.6.....	0.08	0.00	0.01	−0.02	−0.01
K I:					
4250/1.0/1.4.....	0.26	0.14	−0.01	−0.16	0.00
5000/2.5/1.0.....	0.26	0.12	−0.06	−0.07	0.00
Ca I:					
4250/1.0/1.4.....	0.18	0.12	−0.02	−0.10	0.00
5000/2.5/1.0.....	0.13	0.09	−0.03	−0.05	0.00
5500/4.0/0.6.....	0.16	0.08	−0.05	−0.02	−0.01
Sc II:					
4250/1.0/1.4.....	0.20	−0.02	0.07	−0.12	−0.06
5000/2.5/1.0.....	0.12	−0.01	0.08	−0.05	−0.06
5500/4.0/0.6.....	0.10	0.00	0.08	−0.01	−0.05
Ti I:					
4250/1.0/1.4.....	0.16	0.15	0.00	−0.10	0.01
5000/2.5/1.0.....	0.08	0.12	0.00	−0.03	0.01
5500/4.0/0.6.....	0.08	0.09	0.00	−0.01	0.01
V I:					
4250/1.0/1.4.....	0.22	0.18	0.01	−0.12	0.00
5000/2.5/1.0.....	0.09	0.15	0.00	−0.02	0.01
Cr I:					
4250/1.0/1.4.....	0.14	0.10	0.00	−0.09	0.01
5000/2.5/1.0.....	0.08	0.08	0.00	−0.03	0.01
Mn I:					
4250/1.0/1.4.....	0.20	0.08	0.01	−0.07	0.00
5000/2.5/1.0.....	0.12	0.10	0.00	−0.03	0.01
Fe I:					
4250/1.0/1.4.....	0.15	0.03	0.02	−0.09	−0.02
5000/2.5/1.0.....	0.11	0.08	0.00	−0.06	0.00
5500/4.0/0.6.....	0.14	0.08	−0.01	−0.03	0.00
Fe II:					
4250/1.0/1.4.....	0.09	−0.20	0.13	−0.04	−0.09
5000/2.5/1.0.....	0.09	−0.14	0.11	−0.04	−0.08
5500/4.0/0.6.....	0.08	−0.05	0.09	−0.03	−0.05
Co I:					
4250/1.0/1.4.....	0.09	0.04	0.04	−0.02	−0.04
5000/2.5/1.0.....	0.05	0.10	0.01	0.00	−0.01
Ni I:					
4250/1.0/1.4.....	0.20	0.01	0.04	−0.10	−0.04
5000/2.5/1.0.....	0.11	0.07	0.01	−0.06	0.00
5500/4.0/0.6.....	0.13	0.05	0.00	−0.03	−0.01

TABLE 6—*Continued*

Stellar Parameters (1)	ΔW_λ (10%) (2)	$\Delta T_{\rm eff}$ (+100 K) (3)	$\Delta \log(g)$ (+0.2 dex) (4)	$\Delta\xi$ (+0.2 km s^{-1}) (5)	Δ[Fe/H] (+0.2 dex) (6)
Cu I:					
4250/1.0/1.4.....	0.26	0.05	0.05	−0.10	−0.03
5000/2.5/1.0.....	0.13	0.11	0.01	−0.03	0.00
Zn I:					
4250/1.0/1.4.....	0.06	−0.03	0.05	−0.01	−0.02
Y II:					
4250/1.0/1.4.....	0.07	−0.03	0.08	−0.03	−0.06
Zr I:					
4250/1.0/1.4.....	0.13	0.20	0.01	−0.09	0.00
5000/2.5/1.0.....	0.05	0.15	0.00	−0.01	0.01
Ba II:					
4250/1.0/1.4.....	0.23	0.01	0.06	−0.19	−0.08
5000/2.5/1.0.....	0.20	0.02	0.04	−0.16	−0.07
5500/4.0/0.6.....	0.21	0.03	0.03	−0.10	−0.07
La II:					
4250/1.0/1.4.....	0.08	0.01	0.08	−0.04	−0.07
5000/2.5/1.0.....	0.05	0.01	0.08	−0.01	−0.07
Eu II:					
4250/1.0/1.4.....	0.09	−0.02	0.08	−0.06	−0.07
5000/2.5/1.0.....	0.06	0.00	0.08	−0.02	−0.06

[a] Estimated error in the synthesis.

mass asymptotic giant branch (AGB) stars, while Eu is exclusively an *r*-process element.

The abundance ratios of the neutron-capture elements, Y, Zr, Ba, La, and Eu, show no significant trend with $T_{\rm eff}$ and less scatter around the mean than the predicted error, except for [Zr/Fe]. In Figure 9, we show the spectra for two stars of similar $T_{\rm eff}$ and different [Zr/Fe], 1-56 (4525 K, [Zr/Fe] = −0.57) and 1-81 (4550 K, [Zr/Fe] = 0.00) in the region of the Zr line at 6143 Å, which is the strongest Zr I line included in our study. In the spectral range illustrated, there are also two Fe I lines, one Ba II line, and one Si I line, whose strengths are similar in both stars. It is possible but

TABLE 7
MEAN ABUNDANCE RATIOS AND ERRORS

Element (1)	No. of Stars (2)	⟨[X/Fe]⟩ (dex) (3)	$\sigma_{\rm obs}$ (dex) (4)	$\sigma_{\rm pred}$ (dex) (5)	$\Delta_{\rm max}$ (dex) (6)
Li[a]	3	+1.10	0.17	0.13	...
C	6	+1.30[b]	0.49[b]	0.13	1.00 ± 0.37[b]
O	25	+0.19	0.18	0.12	0.48 ± 0.10
Na	25	+0.21	0.13	0.10	0.23 ± 0.11
Mg	24	+0.36	0.09	0.12	0.18 ± 0.07
Al	11	+0.24	0.10	0.10	0.11 ± 0.10
Si	24	+0.28	0.14	0.17	0.19 ± 0.12
K	11	−0.17	0.30	0.29	0.52 ± 0.25
Ca	25	+0.43	0.05	0.11	0.03 ± 0.04
Sc	25	+0.05	0.16	0.15	0.37 ± 0.10
Ti	25	+0.20	0.08	0.11	0.08 ± 0.07
V	21	+0.11	0.14	0.17	0.09 ± 0.08
Cr	23	−0.13	0.09	0.09	0.05 ± 0.05
Mn	13	−0.27	0.11	0.11	0.03 ± 0.08
Co	17	+0.04	0.05	0.10	0.06 ± 0.04
Ni	25	+0.01	0.06	0.09	0.16 ± 0.03
Cu	21	+0.07	0.14	0.21	0.19 ± 0.10
Zn	8	+0.46	0.16	0.22	0.29 ± 0.10
Y	3	−0.22	0.04	0.15	0.06 ± 0.08
Zr	10	−0.14	0.25	0.16	0.61 ± 0.24
Ba	25	+0.34	0.12	0.19	0.03 ± 0.09
La	14	+0.20	0.10	0.15	0.02 ± 0.10
Eu	11	+0.31	0.15	0.15	0.31 ± 0.11

[a] For Li, log ϵ(Li) (H = 12.0 dex) is given. For all other elements, [X/Fe] is given.

[b] The C abundances determined from C I lines in the cooler M71 stars are believed to be spurious due to contamination by lines from the red system of CN.

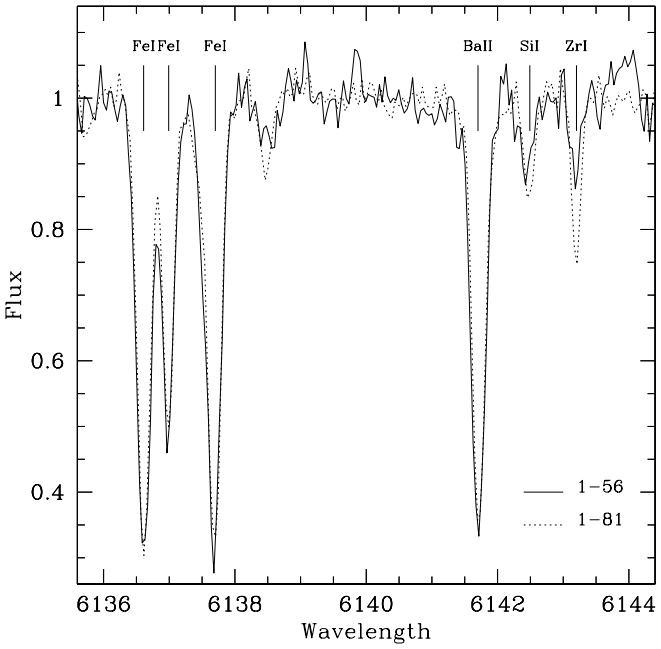

FIG. 9.—Comparison of the strength of the strongest Zr I line included in our study between two stars of similar effective temperatures, 1-56 (4525 K, [Zr/Fe] = −0.57) and 1-81 (4550 K, [Zr/Fe] = 0.00). The scatter shown by [Zr/Fe] might be due to real abundance variations among stars of different $T_{\rm eff}$.

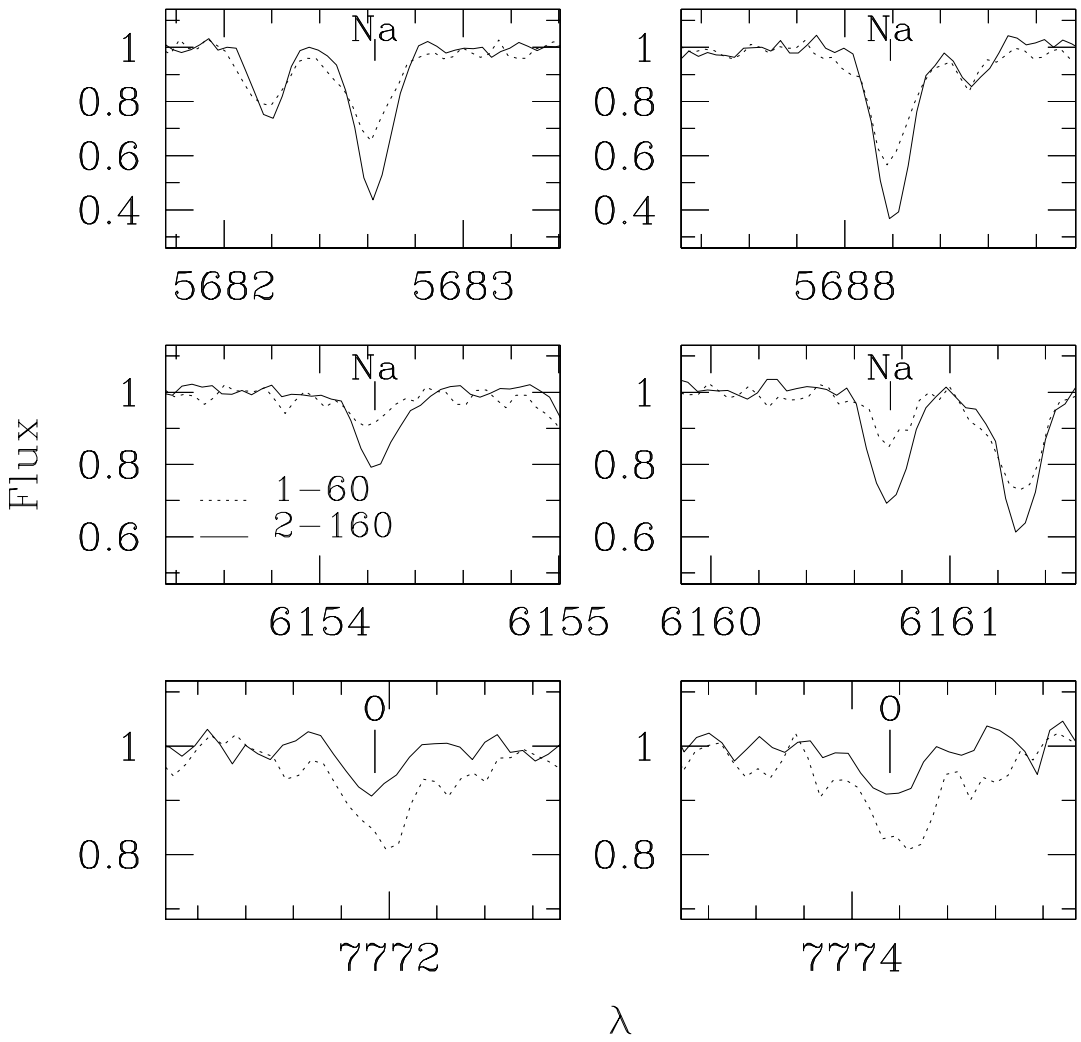

FIG. 10.—Comparison of the strength of four Na I and two O I lines between two stars of similar effective temperatures, 1-60 (4900 K, [Na/Fe] = +0.04, [O/Fe] = +0.33) and 2-160 (5100 K, [Na/Fe] = +0.34, [O/Fe] = +0.06). The scatter shown by [Na/Fe] and [O/Fe] is due to real abundance variations among stars of different $T_{\rm eff}$.

not certain that the difference in strength of the Zr line is due to star-to-star abundance variations. Leep et al. (1987) analyzed four Zr lines in five bright giant M71 stars to obtain [Zr/Fe] $\sim$ 0.0 dex.

The abundances of Ba, La, and Eu are overabundant relative to Fe, as is seen in other clusters (see below). The mean [Ba/Eu] ratio of +0.03 is consistent with values observed in halo stars of similar [Fe/H] (Burris et al. 2000; Gratton & Sneden 1994).

4.3. *α-Elements*

We find that the α-elements Mg, Ca, Si, and Ti are overabundant relative to Fe. Our mean $\langle$[Ti/Fe]$\rangle$ = +0.20 ± 0.08 and $\langle$[Si/Fe]$\rangle$ = +0.28 ± 0.14 are similar to the results of Sneden et al. (1994) for 10 M71 giant stars ($\langle$[Ti/Fe]$\rangle$ = +0.48 ± 0.04, $\langle$[Si/Fe]$\rangle$ = +0.31 ± 0.04) and also similar to the abundance ratios provided by Leep et al. (1987). Our $\langle$[Ca/Fe]$\rangle$ = +0.43 ± 0.05 is higher than the value of Sneden et al. (1994) ($\langle$[Ca/Fe]$\rangle$ = +0.13 ± 0.03), but similar to the abundance ratio of +0.58 found by Leep et al. (1987). The α-element abundance ratios show no significant trend with $T_{\rm eff}$, and low scatter around the mean.

[Mg/Fe] is know to vary among bright giant stars in some metal poor globular clusters. In NGC 6752 (Gratton et al. 2001), M13 (Kraft et al. 1993; Shetrone 1996) and M15 (Sneden et al. 1997), [Mg/Fe] shows a star-to-star range in abundance of about 1.5, 1.2, and 1.0 dex respectively. Our comparison between the observed scatter and the predicted error of [Mg/Fe] given in Table 7 indicates no sign of star-to-star variation of magnesium in M71.

4.4. *Sodium and Oxygen*

The oxygen abundance ratios in our sample of stars in M71 behave differently than the abundance ratios of all other elements included in this paper. The scatter in [O/Fe] versus $T_{\rm eff}$ shown in Figure 3 strongly suggests that O shows star-to-star variations within the M71 sample. Furthermore, the observed scatter for [O/Fe] given in Table 7 is larger than the respective predicted error which include the effects of uncertainties in the determination of the stellar parameters and in the equivalent width measurements. To a lesser extent, the Na abundances behave similarly, as shown in Figure 3, and the observed scatter for Na is slightly larger than the value $\sigma_{\rm pred}$ given in Table 7.

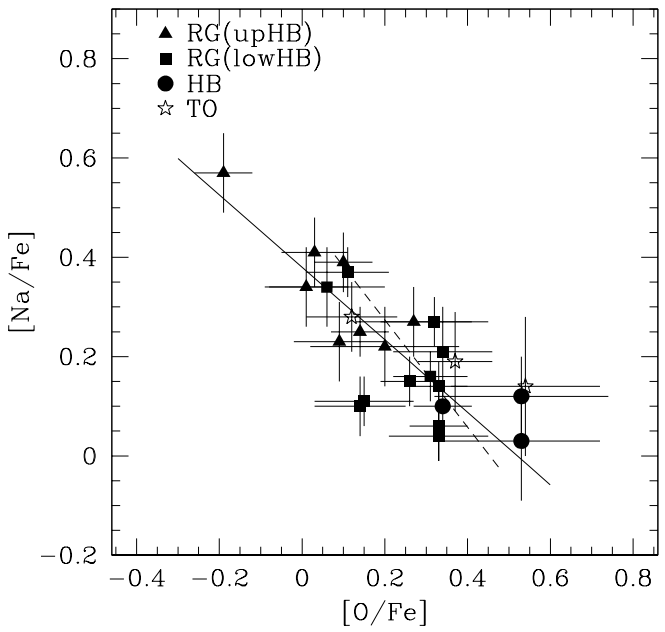

FIG. 11.—[Na/Fe] against [O/Fe] for M71 stars. Filled triangles are RG stars brighter than the HB, filled squares are RG stars fainter than the HB, filled circles are HB stars, and star symbols are stars near the main-sequence turnoff. The solid line represents the least-squares linear fit to our data in M71. The dashed line corresponds to the Na-O anticorrelation present in M4 from the analysis of Ivans et al. (1999).

In Figure 10 we compare the strength of the Na I and O I lines between two stars of similar stellar parameters. The star with a high [O/Fe] in our sample (1-60) has a low [Na/Fe] and the star with a low [O/Fe] (2-160) has an intermediate [Na/Fe]. These two stars are marked with open squares in Figure 3. Note that both of these stars are red giants fainter than the HB, with $M_V = +1.4$ for the fainter, Na-richer star. This figure demonstrates that the higher scatter seen in [Na/Fe] and [O/Fe] is due to star-to-star abundance variations and that in the case of this specific pair of stars, Na and O are anticorrelated, as was first observed by Peterson (1980) in M13.

The non-LTE corrections for the infrared O I triplet are not accurately known (see § 3). However, assuming that they are monotonically dependent on $T_{\rm eff}$, errors in the non-LTE correction cannot introduce a star-to-star scatter in the O abundance nor the Na-O anticorrelation we observe.

To explore the presence of an anticorrelation between [Na/Fe] and [O/Fe] within our M71 sample as a whole, we construct Figure 11, which presents the Na versus O abundance diagram for our sample in M71. Our data are indicated by filled symbols, where triangles are red giants brighter than the HB, circles are HB stars, squares are red giants fainter than the HB, and the stars near the main-sequence turnoff are denoted by star symbols. We find that Na and O are anticorrelated in our sample of M71 stars. The fit weighted by the error of Na versus O, plotted as a solid line in Figure 11, is statistically significant at a $2\,\sigma$ confidence level. Star-to-star Na variations and anticorrelation between Na and O abundances extend well beyond $M_V = +1.4$ and include the small sample of stars near the main-sequence turnoff, where this anticorrelation has the same form as among the more luminous stars and is highly statistically significant at a level exceeding $4\,\sigma$.

In view of the large sample of bright RGB stars studied in M4 by Ivans et al. (1999), we adopt their results for the observed anticorrelation between Na and O among red giants in this cluster to provide a fiducial line for visual comparisons in the relevant figures. The anticorrelation found from their sample is indicated as a dashed line in Figure 11, as well as in the panels of Figure 12, to be discussed next. To within the errors, the Na/O anticorrelation we find in M71 agrees with that of M4, within a $2\,\sigma$ confidence level.

In Figure 12, we compare the determinations of Na and O abundance ratios that exist in the literature for metal poor globular clusters, 47 Tuc (Brown et al. 1990; Brown & Wallerstein 1992; Norris & Da Costa 1995), M71 (Sneden et al. 1994; this paper), M5 (Ivans et al. 2001; Shetrone 1996; Sneden et al. 1992), M4 (Ivans et al. 1999), NGC 6752 (Gratton et al. 2001), M3 (Kraft et al. 1993), M10 (Kraft et al. 1995), M13 (Kraft et al. 1993; Shetrone 1996), NGC 6397 (Castilho et al. 2000; Gratton et al. 2001), M92 (Sneden et al. 1992), and M15 (Sneden et al. 1997). The symbols are the same as in Figure 11. Also included in this figure are the earlier results for ten bright giant stars in M71 from Sneden et al. (1994), shown as open triangles. All their stars are brighter than the HB and behave similarly to our red giants brighter than the HB. Our observed range in [Na/Fe] is similar to the range observed by Sneden et al. (1994), but our range in [O/Fe] is twice as big.

For each globular cluster depicted in Figure 12, the solid line represent the least-squares linear fit of the data from the literature.[4] It is only shown for those globular clusters, where the slope we derive is significant at the $2\,\sigma$ level. The dashed line corresponds to the anticorrelation observed in M4 from Ivans et al. (1999), shown as a fiducial line.

At this confidence level, we find Na-O anticorrelations in M71, M5, M4, NGC 6752, M3, M10, M13, M92, and M15. The steepest slope is that of M92, and the flattest slope is that of M13. But, within the $2\,\sigma$ level, all the slopes are identical.

No statistically significant global anticorrelation is detected in 47 Tuc or NGC 6397.

47 Tuc ([Fe/H] ~ -0.8), M4 ([Fe/H] ~ -1.2) and NGC 6397 ([Fe/H] ~ -2.0) have a similar [Na/Fe] versus [O/Fe] relationship as does M71 does in terms of abundance ratio ranges and scatter. While the form of the relationship appears to be more or less universal, Figure 12 suggests that the amplitude of the Na/O anticorrelation among RGB stars is smallest for the two most metal-rich globular clusters shown, 47 Tuc (where the published data set is very small) and M71, as well as for NGC 6397.

4.5. *Aluminum*

The abundance of Al is also known to vary from star to star within a globular cluster. Because the Al doublet at 6697 Å is not included in the spectral coverage of the primary set of HIRES spectra (see Paper I), it can be measured only in a subset of the sample of stars studied here. Our comparison between $\sigma_{\rm obs}$ and the predicted error of [Al/Fe] given in Table 7 indicates that the scatter for this element

[4] Only for M71 do we use a fit weighted by the errors of each abundance determination; for all other clusters, the errors in the abundance for each star are assumed constant.

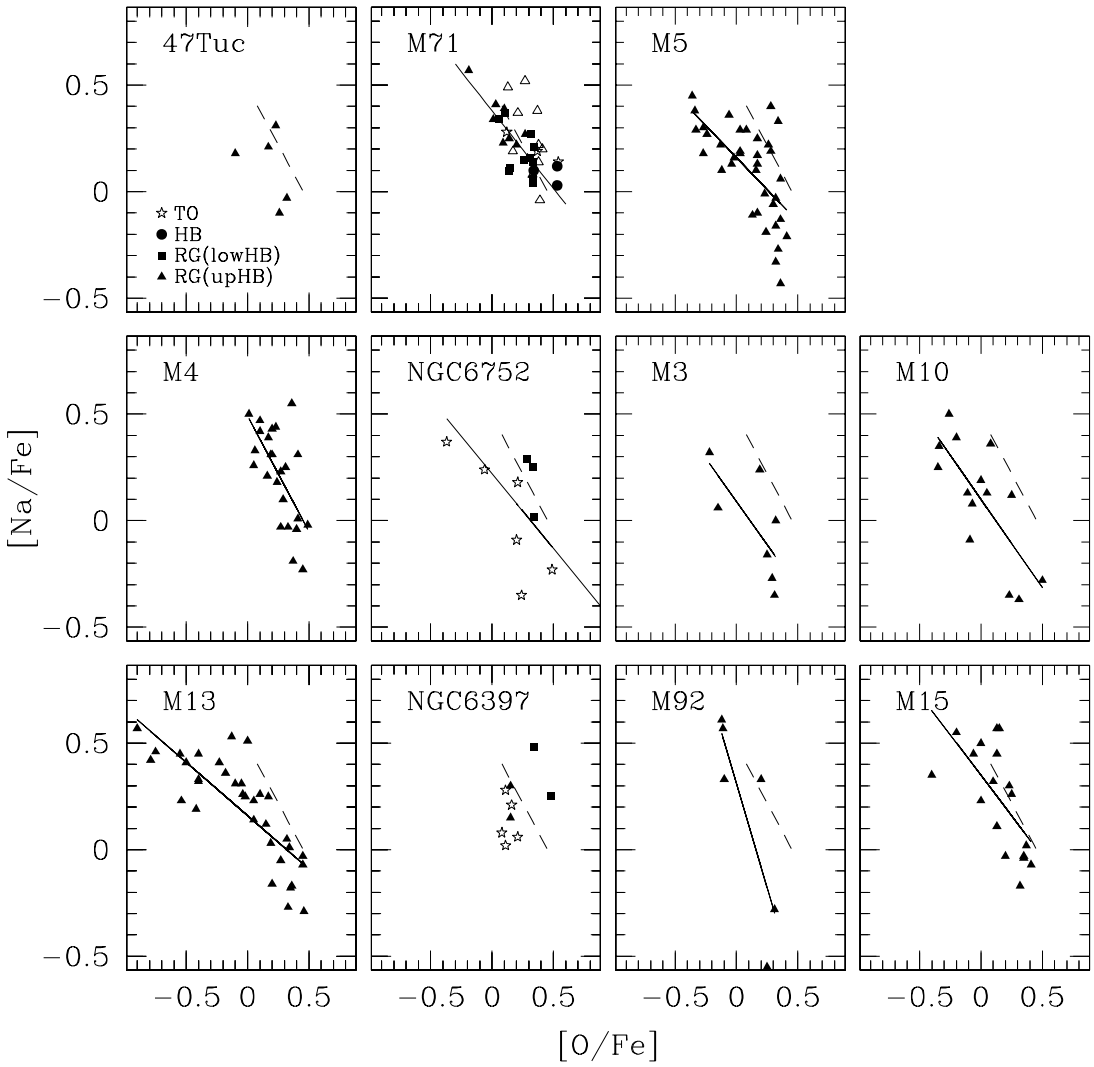

FIG. 12.—[Na/Fe] against [O/Fe] for M71 and for other globular clusters from the literature. Filled symbols are the same as Fig. 11. The literature determinations are: 47 Tuc (Brown et al. 1990; Brown & Wallerstein 1992; Norris & Da Costa 1995), M5 (Ivans et al. 2001; Shetrone 1996; Sneden et al. 1992), M4 (Ivans et al. 1999), NGC 6752 (Gratton et al. 2001), M3 (Kraft et al. 1993), M10 (Kraft et al. 1995), M13 (Kraft et al. 1993; Shetrone 1996), NGC 6397 (Castilho et al. 2000; Gratton et al. 2001), M92 (Sneden et al. 1992), and M15 (Sneden et al. 1997). Open triangles are bright red giants in M71 from the abundance analysis of Sneden et al. (1994). The solid lines represent the least-squares linear fits of the data from the literature for each cluster. They only shown for those globular clusters where the slope we derive is significant at the 2 σ level. The dashed line corresponds to the anticorrelation observed in M4 from Ivans et al. (1999), shown as a fiducial line in each panel.

abundance ratio is slightly larger to its respective predicted error.

As discussed in § 2.5, Al suffers from non-LTE effects. We have not adopted any corrections, nor have we applied any to the set of data from the literature assembled for Al. We do, however, use the 6696 Å doublet, which is less susceptible to non-LTE effects than is the 3961 Å line.

We have constructed Figure 13 to explore the presence of a correlation between [Na/Fe] and [Al/Fe] in M71, seen in other globular clusters. The symbols in Figure 13 are the same as in Figure 11. We include only our own data in this figure. A clear Al/Na correlation is seen which is statistically significant at a 2 σ level. This correlation extends down to $M_V = +1.8$ mag in M71, where the sample ends due to the technical issue of the HIRES spectral coverage.

In Figure 14 we compare the determinations of Al/Na abundance ratios that exist in the literature for metal poor globular clusters. We use the same set of references as in § 4.4, although there are fewer stars with measured Al abundances.

The symbols are the same as in Figure 11. Again the solid line, representing the least squares linear fit of the data, is only shown in those globular clusters where the slope we derive is significant.

At the 2 σ level, we find Na-Al correlations in M5, M4, NGC 6752, M13, NGC 6397, M92, and M15, as well as in M71. At this confidence level, all the slopes, with the exception of that of M13, are identical.

No anticorrelation is detected in 47 Tuc, where the database is very sparse.

The differences among the family of linear fits to the Al/Na relationship for various globular clusters shown in Figure 14 appear at first sight to be considerably larger than those shown by the fits to the Na/O anticorrelation in

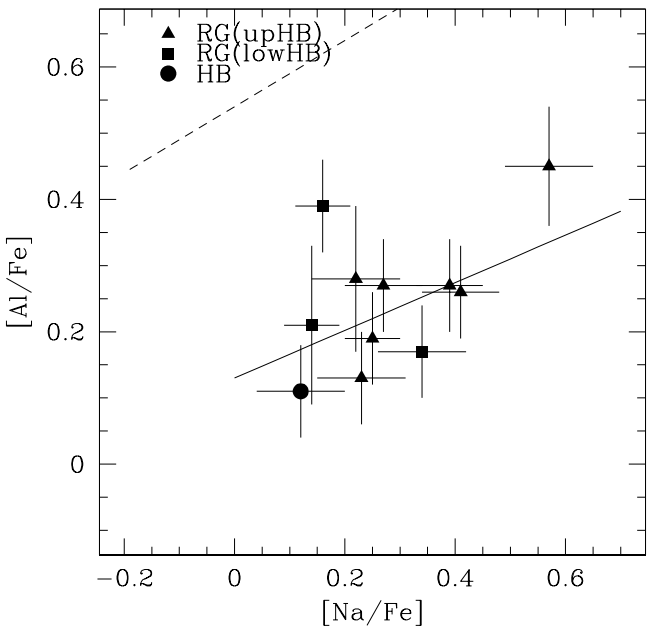

FIG. 13.—[Na/Fe] against [Al/Fe] for M71 stars. Symbols are the same as Fig. 11. The solid line represents the least-squares linear fit to our data in M71. The dashed line corresponds to the Na-Al correlation present in M4 from the analysis of Ivans et al. (1999).

Figure 12. We suggest that these differences may not be real and may arise from non-LTE effects in Al acting on the different ranges of luminosities of stars studied in each cluster, as well as the particular selection of Al lines used in each analysis. The situation in NGC 6752 is particularly illuminating. Gratton et al. (2001) ascribe the very different mean Al abundances deduced for the subgiants and for the main-sequence stars in the cluster precisely to this issue of ignoring non-LTE in the spectrum of aluminum.

4.6. *Lithium*

Li is a very fragile element and is very easily destroyed in stars, burning at $T \gtrsim 2.5 \times 10^6$ K. Spite & Spite (1982) discovered the presence of Li in warm halo dwarfs at a constant value [$\log \epsilon(\mathrm{Li}) = 2.24$] and suggested that this represents the primordial Li synthesized in the big bang and is thus of considerable importance to cosmology. Destruction of Li is a measure of the depth of the surface convection zone and hence a strong function of $T_{\rm eff}$. Ryan et al. (2001) compile recent observations for Li in galactic disk and halo stars and review the Galactic chemical evolution of Li, while Pinsonneault (1997) reviews the destruction of Li from a theoretical perspective.

We therefore expect Li to be depleted among the RGB and subgiant stars in globular clusters, although probably not among the main-sequence stars. In addition, there is at least one case known in a globular cluster of the extremely rare class of very Li-rich stars. A possible explanation for this star, found as a bright RGB star in M3 by Kraft et al. (1999), and similar objects is given by Charbonnel & Balachandran (2000).

The Li line is not included in the spectral coverage of the primary set of spectra (see Paper I) and hence can be measured only in a subset of the sample of M71 stars studied here. We were able to obtain $\log \epsilon(\mathrm{Li})$ for three giants fainter than the HB, as well as several upper limits. The mean $\log \epsilon(\mathrm{Li})$ for the detections is 1.10 ± 0.16 (on the scale $\mathrm{H} = 12.0$ dex), which is 0.8 dex less than the mean $\log \epsilon(\mathrm{Li})$ (1.90 ± 0.42) for a sample of 11 halo dwarf stars of similar [Fe/H] from the sample of Fulbright (2000) and is evidence of the strong depletion among the cooler stars in which Li was detected here. Figure 2 illustrates the pattern of detections and upper limits, which are consistent with our overall expectations.

4.7. *Carbon*

The analysis of C I lines in cool stars is difficult as the lines are weak, and their excitation potential is high, ~8.5 eV. Furthermore, the C I lines near 7115 Å are not included in the spectral coverage of the primary set of spectra (see Paper I) and hence can be measured only in a subset of the sample studied here. We have reliable detections in only six stars, two lines in one star, and one line each in the other five stars. These, with considerable uncertainty, show a large star-to-star scatter in deduced C abundance. However, the C I lines in stars with $T_{\rm eff} \lesssim 4200$ K may be blended with or completely dominated by lines from the red system of CN, as illustrated in the spectrum of Arcturus by Hinkle et al. (2000). It is very likely that this has happened, as there are two cool stars in our sample, M71 1-45 and 1-66, with anomalously high deduced C abundances. The measurements of Briley et al. (2001) show that these two stars have much stronger CN lines than does M71 star I, a star of similar $T_{\rm eff}$ which yielded a much more reasonable C abundance. Unpublished measurements of the *G* band of CH in these three stars by J. G. C. also suggest that the very large C abundances we deduce for M71 1-45 and 1-66 are spurious.

The molecular band data gives a much clearer picture of the pattern of C abundance variation in M71 as the samples are much larger and the C abundance can be inferred with considerable precision from the strength of the CH band. Both the CH and CN bands clearly show strong star-to-star variations on the M71 giant branch (Briley et al. 2001 and references therein) and, more importantly, at the level of the main sequence (Cohen 1999). The entire set of molecular band data can be explained by a variation in C of about a factor of 2, with a much larger anticorrelated variation in the N abundance.

4.8. *Other Clusters*

In Figures 15 to 18, for each element studied here, we provide a comparison to similar high-resolution abundance analyses of halo dwarfs, of RGB stars in M4 ([Fe/H] ~ -1.2), RGB stars in M5 ([Fe/H] ~ -1.2), and RGB stars in M15 from Fulbright (2000), Ivans et al. (1999, 2001), and Sneden et al. (1997), respectively. The halo dwarfs plotted in the figures have been selected from the sample of Fulbright (2000) to have [Fe/H] similar to M71 ($-0.6 <$ [Fe/H] < -0.9). The boxes in Figures 15 to 18 follow the same layout as those in Figure 8. The globular cluster name is indicated above each box ("H" stands for the halo dwarf sample), and the number in parenthesis below the name indicates the number of stars used in the calculation of the respective abundance ratio.

The median abundances for each element determined in each of the five different environments presented in Figures 15 to 18 agree to within the 1 σ uncertainties of

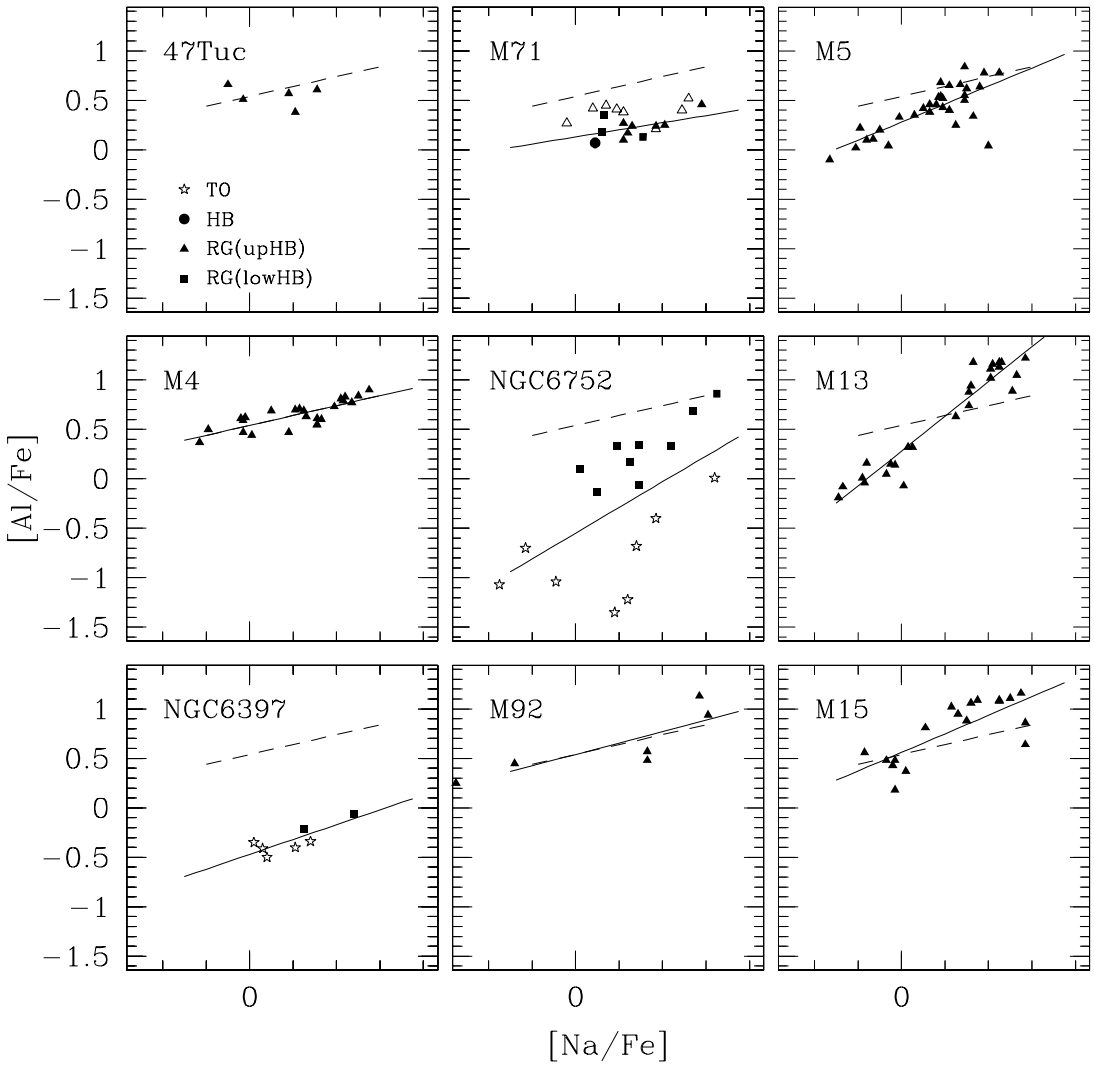

FIG. 14.—[Na/Fe] against [Al/Fe] for other globular clusters from the literature. Filled symbols are the same as Fig. 11. The literature sources used are the same as in Fig. 12. The solid lines represent the least-squares linear fits of the data from the literature for each cluster. They only shown for those globular clusters where the slope we derive is significant at the 2 σ level. The dashed line corresponds to the Na-Al correlation present in M4 from the analysis of Ivans et al. (1999), shown as a fiducial line in each panel.

each measurement for most of the elements displayed, and agree to within ± 1.2 σ for *all* the elements shown. Aluminum is the element showing the largest trend with metallicity between these five environments. This is perhaps a consequence of not considering non-LTE effects and of some studies including the 3961 Å doublet, known to be more sensitive to non-LTE effects, and others not. Barium is the only other element showing large variations in its median abundance among the various environments, although no consistent trend with metallicity. We suggest that this too may not be real and may be a reflection of the issue of hyperfine structure corrections in the fairly strong lines of this element.

Overall M71 appears to have very similar abundance ratios, as does M5. In this set of figures, one can see some of the well-known trends characteristic of halo star abundances as reviewed by McWilliam (1997), such as the gradual increase of [α/Fe] as [Fe/H] decreases, particularly for Si and Ti.

4.9. *Interpretation*

A classical review of post–main-sequence stellar evolution can be found in Iben & Renzini (1983). Their description of the consequences of the first dredge-up phase, the only dredge-up phase any of the stars in our M71 sample may have experienced, indicates that a doubling of the surface N^{14} and a 30% reduction in the surface C^{12} can be expected, together with a drop in the ratio of C^{12}/C^{13} from the solar value of 89 to $\sim$20, as well as a drop in surface Li and B by several orders of magnitude. Observations of field stars over a wide range of luminosities conform fairly well to this picture (see, e.g., Shetrone et al. 1993; Gratton et al. 2000).

However, the O/Na anticorrelation seen among the bright red giants in many globular clusters, including here in the case of M71, cannot be explained in this picture. Several theoretical mechanisms have thus been proposed (e.g., the meridional mixing of Sweigart & Mengel 1979 and turbu-

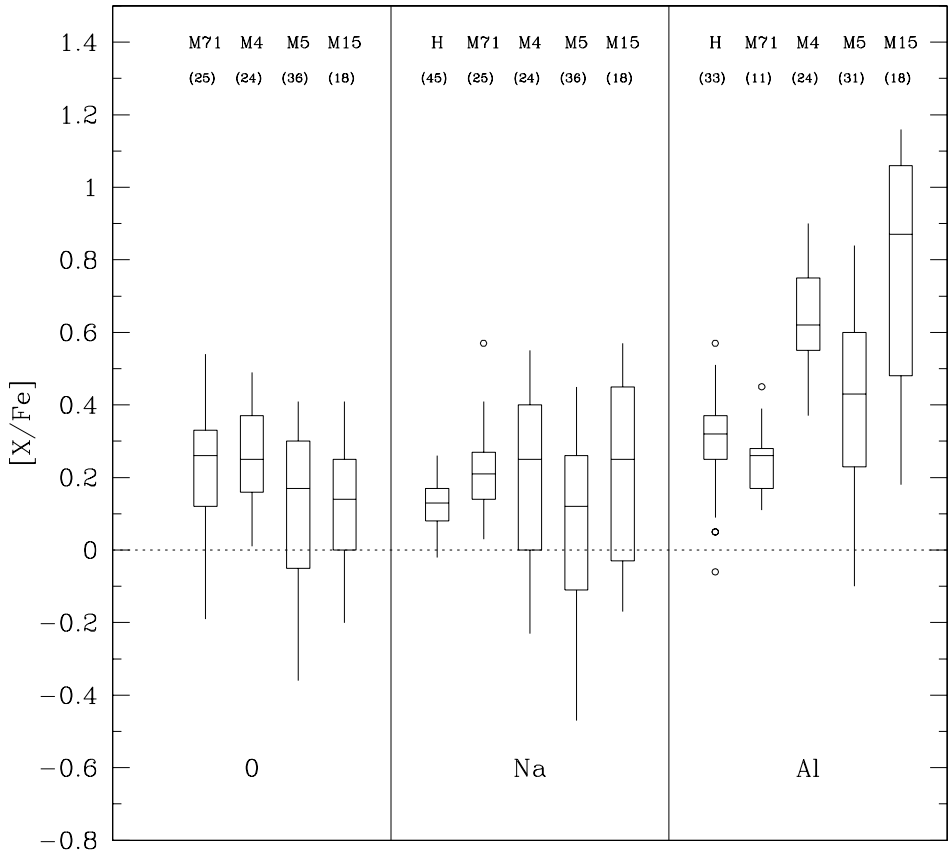

FIG. 15.—Statistical comparison of light elements with median abundances from halo dwarfs, M4 ([Fe/H] ~ -1.2), M5 ([Fe/H] ~ -1.2), and M15 from Fulbright (2000), Ivans et al. (1999, 2001), and Sneden et al. (1997), respectively. The halo dwarfs plotted in the figures have been selected from the sample of Fulbright (2000) to have [Fe/H] similar to M71 ($-0.6 <$ [Fe/H] < -0.9). The number in parenthesis indicates the number of stars analyzed for each element in the corresponding globular cluster. The layout of the statistical box for each element is as in Fig. 8.

lent diffusion of Charbonnel 1994, 1995) with varying degrees of success. In addition, Denisenkov & Denisenkova (1990) suggested that the nuclear reaction $^{22}\mathrm{Ne}(p,\gamma)^{23}\mathrm{Na}$ occurs in regions of the H-burning shell for low-mass stars where O is converted into N and produces Na^{23} and Al^{27}. Langer et al. (1993) combined these ideas to predict the consequences of such possible synthesis and deep mixing, including for example, that the surface Mg abundance should be much less affected than that of Na or Al. These ideas form the basis of our current understanding of dredge up in low mass metal poor giants, with more recent calculations given by Denissenkov & Weiss (1996), Cavallo et al. (1998), andWeiss et al. (2000), among others.

The clear prediction of this suite of calculations is that the earliest that deep mixing can begin is at the location of the bump in the luminosity function of the RGB, which occurs when the H-burning shell crosses a sharp chemical discontinuity. Zocalli et al. (1999) have shown that the luminosity of the RGB bump as a function of metallicity as determined from observation agrees well with that predicted by the theory of stellar evolution. Bono et al. (2001) further suggest that the agreement between the predicted luminosity function and actual star counts along the RGB in the vicinity of the bump in a suite of globular clusters is so good that mixing (more exactly, mixing of He) cannot have occurred any earlier, otherwise the evolutionary lifetimes, and hence the observed LF, of such stars would have been affected.

Our sample of M71 stars shows a statistically significant correlation between Al and Na abundances which extends to stars as faint as $M_V = +1.8$ mag. We also see an anticorrelation between the Na and O abundances extending down to near the main-sequence turnoff. We see variations in Li (as expected) and may see variations in Zr (not expected). Any variations in Mg are smaller than those of Al, Na, or O (as expected). We know there are large anticorrelated C and N variations from the work of Cohen (1999); this too is expected.

The behavior of Li, which is very fragile and easily destroyed, is not controversial. It is, however, the range of luminosity over which the remainder of these variations are seen which is becoming more and more of a problem for any scenario that invokes dredge-up and mixing. The Na/O anticorrelation we see in M71 extends to the main-sequence turnoff. The Al/Na correlation we see in M71 extends to at least as faint as $M_V = +1.8$, while the RGB bump in a cluster of the metallicity of M71 is at $M_V = +1.0$. Cohen (1999) has shown that the C/N anticorrelation extends to the stars at the main-sequence turnoff and even fainter in M71. Briley & Cohen (2001) have shown that the C/N abundance range seen at the level of the main sequence is comparable to that seen among the bright red giants of M71 by many previous studies, the most recent of which is Briley et al. (2001).

The accumulated weight of recent evidence, both in M71 as described above and in other globular clusters, such as 47

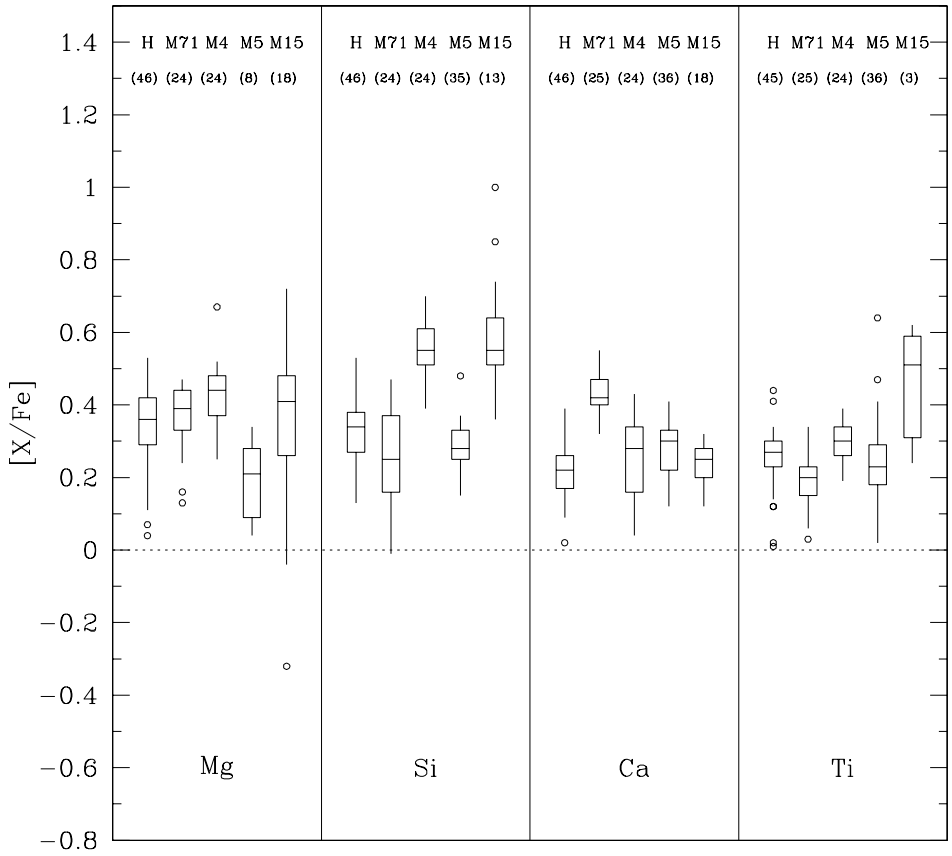

FIG. 16.—Statistical comparison of the abundance of α-elements in various environments. Symbols and references as in Fig. 15.

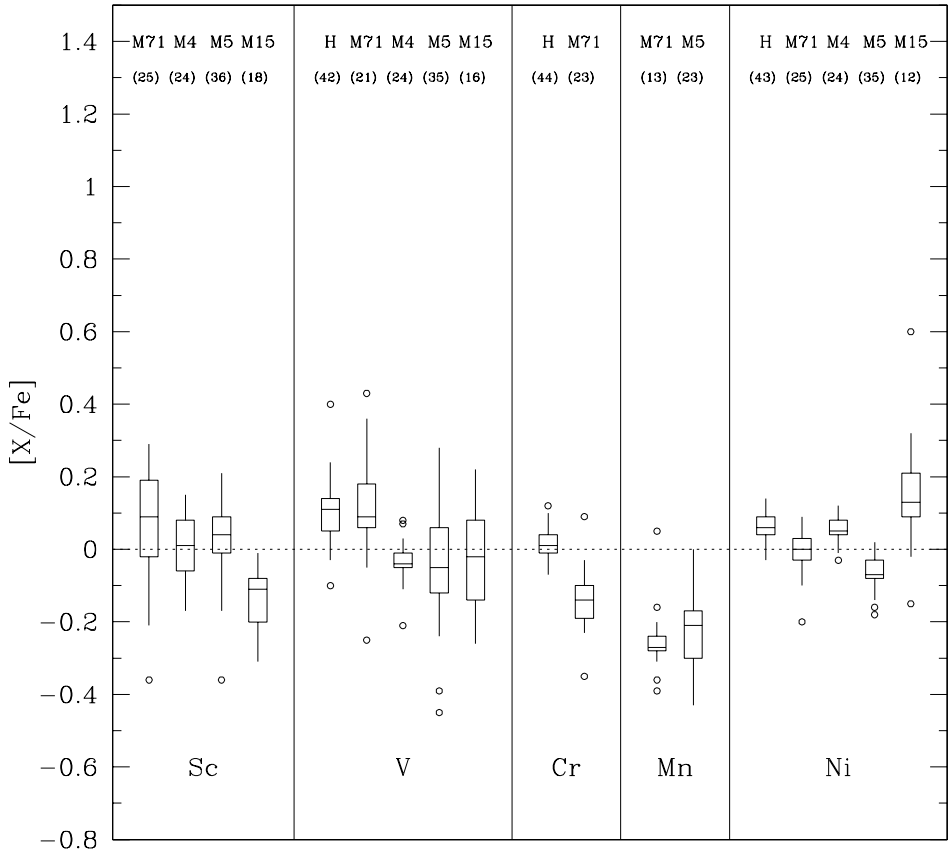

FIG. 17.—Statistical comparison of the abundance of iron peak elements in various environments. Symbols and references as in Fig. 15.

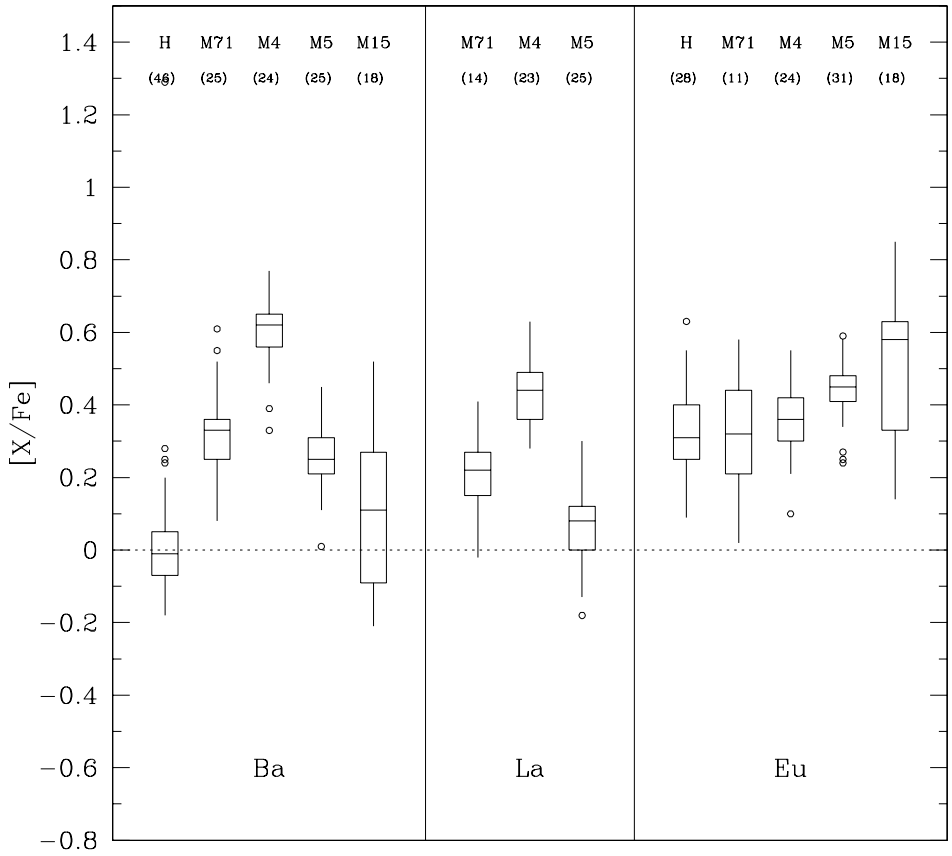

FIG. 18.—Statistical comparison of the abundance of neutron-capture elements in various environments. Symbols and references as in Fig. 15.

Tuc (see Cannon et al. 1998 and references therein) and NGC 6752 (see Gratton et al. 2001 and references therein), suggests that we are now back in the situation we were during the late 1980s. Unless we have missed some important aspect of stellar evolution with impact on mixing and dredge up, we must declare the mixing scenario a failure for the specific case of M71 (and several other globular clusters as well). Even the theoreticians in the forefront of this field are beginning to admit that deep mixing alone is not sufficient (Denissenkov & Weiss 2001; Ventura et al. 2001). Unless and until some major new concept relevant to this issue appears, we must now regard the fundamental origin of the star-to-star variations we see in M71 as arising outside the stars whose spectra we have studied here.

5. CONCLUSIONS

We present results of a high dispersion analysis of 23 elements to obtain abundance ratios for 25 members of the Galactic globular cluster M71. Our sample of stars includes 19 giant stars (nine of which are less luminous than the RHB), three horizontal branch stars, and three stars near the main-sequence turnoff. Our conclusions are summarized as follows:

1. The iron peak and neutron-capture element abundance ratios show no trend with $T_{\rm eff}$ and low scatter around the mean.

2. The α-elements Mg, Ca, Si, and Ti are overabundant relative to Fe. The scatter about the mean is small.

3. An anticorrelation between the Na and O abundances for stars in M71 is detected with a statistical significance in excess of 2 σ and extends to the stars near the main-sequence turnoff.

4. The [Na/Fe] versus [Al/Fe] correlation is detected with a statistical significance in excess of 2 σ in our sample of M71 stars and extends at least as faint as $M_V = +1.8$.

5. Neither extremely O-poor, Na-rich stars or extremely O-rich, Na-poor stars such as are observed in M5 and in M13 are present in our sample of M71 stars.

6. Li is varying among the subgiants (as expected), and Zr may be varying among the subgiants.

M71 appears very similar in its element abundance ratios to M5, which is not surprising as M5 has a metallicity only slightly lower, [Fe/H] $= -1.2$ dex (Ivans et al. 2001). However, the amplitude of the Na/O and Al/Na relationships appears to be somewhat larger in M5 than in M71, and still larger in even more metal poor clusters.

Our detailed abundance analysis of 25 stars in M71 has revealed abundance variations appearing at such low luminosities that deep mixing scenarios can no longer reproduce these results. This problem is made even more acute when we add in the data of Cohen (1999) and the analysis of Briley & Cohen (2001) of the CH and CN bands in M71. We are forced to the firm conclusion that much, if not all, of the abundance variations seen in M71 must have been in place before the present generation of stars we observe was formed, or (less likely) are the result of some type (binaries?) of mass transfer.

In future papers we will proceed to apply the techniques and analysis developed here for M71 to other more metal poor globular clusters, where the RGB bump is predicted to be somewhat more luminous and where, judging from the behavior of their bright RGB stars, we may anticipate finding even larger variations at low luminosities among the cluster subgiants and main-sequence stars.

The entire Keck/HIRES user communities owes a huge debt to Jerry Nelson, Gerry Smith, Steve Vogt, and many other people who have worked to make the Keck Telescope and HIRES a reality and to operate and maintain the Keck Observatory. We are grateful to the W. M. Keck Foundation for the vision to fund the construction of the W. M. Keck Observatory. The authors wish to extend special thanks to those of Hawaiian ancestry on whose sacred mountain we are privileged to be guests. Without their generous hospitality, none of the observations presented herein would have been possible. We are grateful to the National Science Foundation for partial support under grant AST-98 19614 to J. G. C. We thank Jason Prochaska and Andy McWilliam for providing their tables of hyperfine structure in digital form.

REFERENCES

Allende Prieto, C., Lambert, D. L., & Asplund, M. 2001, ApJ, 556, L63
Arp, H. C., & Hartwick, F. D. A. 1971, ApJ, 167, 499
Anders, E., & Grevesse, N. 1989, Geochim. Cosmochim. Acta, 53, 197
Baumüller, D., Butler, K., & Gehren, T. 1998, A&A, 338, 637
Baumüller, D., & Gehren, T. 1996, A&A, 307, 961
———. 1997, A&A, 325, 1088
Bono, G., Cassisi, S., Zocalli, M., & Piotto, G. 2001, ApJ, 546, L109
Briley, M. M., & Cohen, J. G. 2001, AJ, 122, 242
Briley, M. M., Smith, G. H., & Claver, C. F. 2001, AJ, 122, 2561
Brown J. A., Wallerstein, G., & Oke, J. B. 1990, AJ, 100, 1561
Brown J. A., & Wallerstein, G. 1992, AJ, 104, 1818
Burris, D. L., Pilachowski, C. A., Armandroff, T. E., Sneden, C., Cowan, J. J., & Roe, H. 2000, ApJ, 544, 302
Cameron, A. G. W. 1982, Ap&SS, 82, 123
Cannon, R. D., Croke, B. F. W., Bell, R. A., Hesser, J. E., & Stathakis, R. A. 1998, MNRAS, 298, 601
Castilho, B. V., Pasquini, L., Allen, D. M., Barbuy, B., & Molaro, P. 2000, A&A, 361, 92
Cavallo, R. M., Sweigart, A. V., & Bell, R. A. 1998, ApJ, 492, 575
Charbonnel, C. 1994, A&A, 282, 811
———. 1995, ApJ, 453, L41
Charbonnel, C., & Balachandran, S. C. 2000, A&A, 359, 563
Cohen, J. G. 1983, ApJ, 270, 654
———. 1999, AJ, 117, 2434
Cohen, J. G., Behr, B. B., & Briley, M. M. 2001, AJ, 122, 1420 (Paper I)
de la Reza, R., & Muller, E. A. 1975, Sol. Phys., 43, 15
Denisenkov, P. A., & Denisenkova, S. N. 1990, Soviet Astron. Lett., 16, 275
Denissenkov, P. A., & Weiss, A. 1996, A&A, 308, 773
———. 2001, ApJ, 559, L115
Fuhr, J. R., Martin, G. A., & Wiese, W. L. 1988, J. Phys. Chem. Ref. Data 17, Suppl. 4
Fulbright, J. 2000, AJ, 120, 1841
Gratton, R. G., et al. 2001, A&A, 369, 87
Gratton, R. G., Carretta, E., Eriksson, K., & Gustafsson, B. 1999, A&A, 350, 955
Gratton, R. G., Quarta, M. L., & Ortolani, S. 1986, A&A, 169, 208
Gratton, R. G., & Sneden, C. 1994, A&A, 287, 927
Gratton, R. G., Sneden, C., Carretta, E., & Bragaglia, A. 2000, A&A, 354, 169
Hinkle, K., Wallace, L., Valenti, J., & Harmer, D. 2000, Visible and Near-Infrared Atlas of the Arcturus Spectrum, 3727–9000 Å (San Francisco: ASP)
Holweger, H., Bard, A., Kock, A., & Kock, M. 1991, A&A, 249, 545
Iben, I., Jr. & Renzini, A. 1983, ARA&A, 21, 271
Israelian, G., Rebolo, R., García López, R. J., Bonifacio, P., Molaro, P., Basri, G., & Shchukina, N. 2001, ApJ, 551, 833
Ivans, I. I., Kraft, R. P., Sneden, C., Smith, G., Rich, R. M., & Shetrone, M. 2001, AJ, 122, 1438
Ivans, I. I., Sneden, C., Kraft, R. P., Suntzeff, N. B., Smith, V. V., Langer, G. E., & Fulbright, J. P. 1999, ApJ, 118, 1273
Johnson, J. 2002, ApJS, 139, 219
Käppeler, F., Beer, H., & Wisshak, K. 1989, Rep. Prog. Phys., 52, 945
Kraft, R. P. 1994, PASP, 106, 553
Kraft, R. P., Sneden, C., Langer, G. E., & Shetrone, M. D. 1993, AJ, 106, 1490
Kraft, R. P., Sneden, C., Langer, G. E., Shetrone, M. D., & Bolte, M. 1995, AJ, 109, 2586
Kraft, R. P., Peterson, R. C., Puragra, G., Sneden, C., Fulbright, J. P., & Langer, G. E. 1999, ApJ, 518, L53
Kurucz, R. L. 1993a, CD-ROM 13, ATLAS9 Stellar Atmosphere Programs and 2 km/s Grid (Cambridge: Smithsonian Astrophys. Obs.)
———. 1993b, CD-ROM 18, SYNTHE Spectrum Synthesis Programs and Line Data (Cambridge: Smithsonian Astrophys. Obs.)
Lambert, D. L. 2002, Highlights Astron., in press
Langer, G. E., Hoffman, R., & Sneden, C. 1993, PASP, 105, 301
Leep, E. M., Oke, J. B., & Wallerstein, G. 1987, AJ, 93, 338
Martin, G. A., Fuhr, J. R., & Wiese, W. L. 1988, J. Phys. Chem. Ref. Data, 17, suppl. 3
McWilliam, A. 1997, ARA&A, 35, 503
Meléndez, J., Barbuy, B., & Spite, F. 2001, ApJ, 556, 858
Moore, C. E., Minnaert, M. G. J., & Houtgast, J. 1966, The Solar Spectrum 2935 Å to 8770 Å (Washington: GPO)
Norris, J. E., & Da Costa, G. S. 1995, ApJ, 447, 680
Peterson, R. C. 1980, ApJ, 237, L87
Pinsonneault, M. 1997, ARA&A, 35, 557
Prochascka, J. X., Naumov, S. O., Carney, B. W., McWilliam, A., & Wolfe, A. M. 2000, AJ, 120, 2513
Ramírez, S. V., Cohen, J. G., Buss, J., & Briley, M. M. 2001, AJ, 122, 1429
Ryan, S. G., Kajino, T., Beers, T. C., Suzuki, T. K., Romano, D., Matteucci, F., & Rosolankova, K. 2001, ApJ, 549, 55
Shetrone, M. D. 1996, AJ, 112, 1517
Shetrone, M. D., Sneden, C., & Pilachowski, C. A. 1993, PASP, 105, 337
Smith, G., & Raggett, D. St. J. 1981, J. Phys. B, 14, 4015
Sneden, C. 1973, Ph.D. thesis, Univ. Texas
Sneden, C., Kraft, R. P., Langer, G. E., Prosser, C. F., & Shetrone, M. D. 1992, AJ, 104, 2121
Sneden, C., Cowan, J. J. & Truran, J. W. 2001, in Cosmic Evolution, ed. E. Vangioni-Flam, R. Ferlet, & M. Lemoine (Singapore: World Sci.), 179
———. 1994, AJ, 107, 1773
———. 1997, AJ, 114, 1964
Spite, F., & Spite, M. 1982, A&A, 115, 357
Sweigart, A. V., & Mengel, J. G. 1979, ApJ, 229, 624
Takeda, Y. 2002, ApJ, submitted (astro-ph/0105215)
Takeda, Y., Zhao, G., Chen, Y., Qiu, H., & Takada-Hidai, M. 2000, PASJ, in press
Thévenin, F. 1989, A&AS, 77, 137
———. 1990, A&AS, 82, 179
Ventura, P., D'Antona, F., Mazzitelli, I. & Gratton, R. 2001, ApJ, 550, L65
Wallace, L., Hinkle, K. & Livingston, W. C. 1998, An Atlas of the Spectrum of the Solar Photosphere from 13,500 to 28,000 cm^{-1}
Wiese, W. L., Fuhr, J. R., & Deters, T. M. 1996, J. Phys. Chem. Ref. Data, Monogr. 7
Wiese, W. L., Smith, M. W., & Miles, B. M. 1969, Atomic Transition Probabilities, Volume 2 (NSRDS-NBS 22) (Washington: GPO)
Weiss, A., Denissenkov, P. A., & Charbonnel, C. 2000, A&A, 356, 181
Zhao, G., Butler, K., & Gehren, T. 1998, A&A, 333, 219
Zocalli, M., Cassisi, G., Piotto, G., Bono, G., & Salaris, M. 1999, ApJ, 518, L49